

# EVALUATION OF INTERFEROMETRIC SYNTHETIC APERTURE RADAR (InSAR) TECHNIQUES FOR MEASURING LAND SUBSIDENCE AND CALCULATED SUBSIDENCE RATES FOR THE ESCALANTE VALLEY, UTAH, 1998 TO 2006

*by Richard R. Forster*



**OPEN-FILE REPORT 589**  
**UTAH GEOLOGICAL SURVEY**  
*a division of*  
**UTAH DEPARTMENT OF NATURAL RESOURCES**  
**2012**

# EVALUATION OF INTERFEROMETRIC SYNTHETIC APERTURE RADAR (InSAR) TECHNIQUES FOR MEASURING LAND SUBSIDENCE AND CALCULATED SUBSIDENCE RATES FOR THE ESCALANTE VALLEY, UTAH, 1998 TO 2006

*by Richard R. Forster*  
*Geography Department*  
*University of Utah*



**OPEN-FILE REPORT 589**  
**UTAH GEOLOGICAL SURVEY**  
*a division of*  
UTAH DEPARTMENT OF NATURAL RESOURCES  
**2012**

**STATE OF UTAH**

Gary R. Herbert, Governor

**DEPARTMENT OF NATURAL RESOURCES**

Michael Styler, Executive Director

**UTAH GEOLOGICAL SURVEY**

Richard G. Allis, Director

**PUBLICATIONS**

contact

Natural Resources Map & Bookstore

1594 W. North Temple

Salt Lake City, UT 84116

telephone: 801-537-3320

toll-free: 1-888-UTAH MAP

website: [mapstore.utah.gov](http://mapstore.utah.gov)

email: [geostore@utah.gov](mailto:geostore@utah.gov)

**UTAH GEOLOGICAL SURVEY**

contact

1594 W. North Temple, Suite 3110

Salt Lake City, UT 84116

telephone: 801-537-3300

website: [geology.utah.gov](http://geology.utah.gov)

*This open-file release was prepared by the author under contract to the Utah Department of Natural Resources, Utah Geological Survey. The report has not undergone the full UGS review process, and may not conform to UGS technical, editorial, or policy standards. Therefore, it may be premature for an individual or group to take action based on the contents of this report.*

*The Utah Department of Natural Resources, Utah Geological Survey, makes no warranty, expressed or implied, regarding the suitability of this product for a particular use. The Utah Department of Natural Resources, Utah Geological Survey, shall not be liable under any circumstances for any direct, indirect, special, incidental, or consequential damages with respect to claims by users of this product.*

# CONTENTS

ABSTRACT.....	1
INTRODUCTION .....	1
Objective.....	1
Persistent Scatterer Interferometric Synthetic Aperture Radar (PSInSAR) Theory .....	1
Data Set.....	2
PROCESSING.....	2
Traditional InSAR and Persistent Scatterer InSAR.....	2
Persistent Scatterer InSAR.....	4
PSInSAR RESULTS .....	5
INVESTIGATION OF PS LOCATIONS.....	6
RECENT DEFORMATION MAPS FROM TRADITIONAL INSAR.....	12
Phase unwrapping procedure.....	12
Subsidence maps.....	13
CONCLUSIONS AND RECOMMENDATIONS .....	24
ACKNOWLEDGMENTS.....	24
REFERENCES.....	24

## FIGURES

Figure 1. Southwest corner of Utah with blue box indicating approximate location of the SAR frame .....	3
Figure 2. SAR image of Escalante Valley, Utah, representing mean backscatter for 32 ERS-1/2 scenes.....	5
Figure 3. Phase of candidate persistent scatterers shown with color over SAR image of Escalante Valley.....	6
Figure 4. SAR image of Escalante Valley, Utah, representing mean backscatter for 32 ERS-1/2 scenes .....	7
Figure 5. a) SAR image with yellow dots as candidate persistent scatterers. Subset of figure 2. b) Portion of digital orthorectified aerial photograph taken in 1983.....	8
Figure 6. Subsets of figure 5. a) SAR image with yellow dots as candidate persistent scatterers. b) Portion of digital orthorectified aerial photograph taken in 1983.....	8
Figure 7. Photographs of features north of Beryl Junction labeled in figure 6 taken on 6/19/2007 .....	9
Figure 8. Photographs of persistent scatterer clusters at Beryl Junction labeled in figure 6 taken on 6/19/2007.....	9
Figure 9. Photographs of a persistent scatterer cluster south of Beryl Junction labeled in figure 5 taken on 6/19/2007....	10
Figure 10. Power lines northeast of Newcastle.....	11
Figure 11. Photographs of features that were not classified as candidate persistent scatterer clusters in the Escalante Valley taken on 6/19/2007 .....	11
Figure 12. Series of SAR images of the Escalante Valley.....	12
Figure 13a. Vertical displacement map of the Escalante Valley from InSAR pair 4/21/1998-11/2/1999 .....	14
Figure 13b. Vertical displacement map of the Escalante Valley from InSAR pair 11/2/1999-10/17/2000 .....	15
Figure 13c. Vertical displacement map of the Escalante Valley from InSAR pair 10/26/2004-11/15/2005.....	16
Figure 13d. Vertical displacement map of the Escalante Valley from InSAR pair 10/11/2005-12/5/2006.....	17
Figure 14a. Subsidence rate map of the Escalante Valley from InSAR pair 4/21/1998-11/2/1999 .....	18
Figure 14b. Subsidence rate map of the Escalante Valley from InSAR pair 11/2/1999-10/17/2000.....	19
Figure 14c. Subsidence rate map of the Escalante Valley from InSAR pair 10/26/2004-11/15/2005.....	20
Figure 14d. Subsidence rate map of the Escalante Valley from InSAR pair 10/11/2005-12/5/2006 .....	21
Figure 15a. Change in subsidence rate of the Escalante Valley from subtracting figure 14b .....	22
Figure 15b. Acceleration of subsidence in the Escalante Valley from subtracting figure 14b .....	23

## TABLES

Table 1. Synthetic aperture radar (SAR) data used in this study.....	4
Table 2. Interferometric pairs used to make displacement maps.....	12

# EVALUATION OF INTERFEROMETRIC SYNTHETIC APERTURE RADAR (InSAR) TECHNIQUES FOR MEASURING LAND SUBSIDENCE AND CALCULATED SUBSIDENCE RATES FOR THE ESCALANTE VALLEY, UTAH, 1998 TO 2006

by *Richard R. Forster*

## ABSTRACT

Previous studies have shown the Escalante Valley, Utah, is subsiding due to groundwater withdrawal. The magnitude and spatial pattern of this cm/yr.-scale subsidence is mapped with satellite data from a synthetic aperture radar (SAR) using interferometric SAR (InSAR) processing techniques. A relatively new processing approach that measures individual pixel displacements for selected persistent scatterers (PSInSAR) is tested in the agricultural setting of the Escalante Valley. The PSInSAR technique, which is typically used in urban environments, was unsuccessful in this setting due to too few and too widely spaced persistent scatterers, such as metal buildings surrounded by gravel/bare ground and metal power line towers. Four nearly annual subsidence rate maps spanning 1998 to 2006 were successfully produced using traditional InSAR processing from ERS-2 and ENVISAT satellites. Maximum subsidence rates are typically 6 cm/yr. From 1998 to 2006 the extent of subsidence expanded and the subsidence rates accelerated in most areas, although subsidence surrounding some water wells decelerated. The projected accumulated subsidence from 1998 to 2016 for the areas of maximum subsidence is greater than one meter. Continual acquisition and analysis of SAR data can be used to map future subsidence and as a tool to measure changes in subsidence for evaluation of mitigation strategies.

## INTRODUCTION

### Objective

The objectives of this study are to 1) test the suitability of a relatively new application of interferometric synthetic

aperture radar (InSAR) and 2) use traditional InSAR to measure land surface subsidence in the Escalante Valley, Utah. The new technique, persistent scatterer InSAR (PSInSAR), allows subsidence to be measured over longer time periods and greater spatial extents than the traditional InSAR technique (Ferretti and others 2001). The Utah Geological Survey (UGS) documented earth fissures near Beryl Junction in Iron County, Utah, during the winter of 2004/2005 (Lund and others, 2005). The UGS study determined that these fissures were the result of compaction in the Escalante Valley aquifer due to groundwater withdrawal (Lund and others, 2005). This study will test the applicability of PSInSAR to measure the surface deformation history of the area from 1993 to 2007 and produce subsidence maps using traditional InSAR from 1998 to 2006.

A previous study demonstrated that traditional InSAR could be used to map subsidence rates in the Escalante Valley from 1993 to 1998 (Forster, 2006). Maximum rates of 3-4 cm/yr. were found where the InSAR measurement was possible. This did not include the central portion of the valley due to limitations of the previous processing techniques.

### Persistent Scatterer Interferometric Synthetic Aperture Radar (PSInSAR) Theory

Synthetic aperture radar (SAR) uses the amplitude of microwave pulses reflected from the ground surface to generate images depicting roughness and dielectric characteristics of the surface. These imaging SARs do not look straight down from the satellite like most remote sensing imagery. A SAR always looks to one side of the satellite to form its image. This is required since the travel time of the radar pulse is used to locate the return signal in the image and there would be an ambiguity as to which side the returned signal came from if the radar were looking

straight down and illuminating both sides of the satellite track. Therefore, the energy received at the radar must be scattered back in the same direction it was transmitted. This energy is sometimes referred to as *backscatter*. Since SAR uses a coherent signal processing technique, phase as well as the amplitude of the backscatter for each pixel is recorded. Interferometric SAR (InSAR) uses the difference in phase between two repeat-pass scenes to effectively measure the difference in path length (Rosen and others, 2000). If the distance between the satellite positions during the repeat-pass (the baseline) is accurately known and digital topography is available, then sub-centimeter changes in the ground surface elevation can be measured. The time lapse between the acquisitions can be days to years. After InSAR processing, the pixels represent approximately 30-meter squares. Traditional InSAR requires the radar-scattering properties of large contiguous areas (hundreds of pixels) to remain consistent over the time span between SAR acquisitions (Rosen and others, 2000).

Traditional InSAR derived surface displacements have been used to measure the effects of overstressed aquifers in a variety of urban settings, for example: Antelope Valley, California (Galloway and others 1998), Las Vegas, Nevada (Amelung and others 1999), San Jose, California (Galloway and others, 2000), Bologna, Italy, and Mexico City, Mexico (Strozzi and others, 2003). Seasonal-scale subsidence and rebound due to summer ground water extraction and spring recharge of aquifers have also been measured with InSAR in Los Angeles (Bawden and others, 2001), Las Vegas (Hoffmann and others 2001), and San Bernardino (Lu and Danskin, 2001).

A more recent InSAR technique, persistent scatterers (PSInSAR), uses the phase information from only individually selected pixels that exhibit stable radar scattering properties (Ferretti and others, 2001). In urban areas strong stable radar returns from buildings, houses, and other built structures result in millions of PS pixels per SAR scene. These PS pixels have stable radar scattering properties over many years; thus, a sequence of SAR images can be used to produce a long-time series of surface displacement measurements for thousands of individual points. Each PS point can be thought of as a permanent GPS location with a monthly sampling frequency. The PSInSAR technique has the additional benefit of reducing atmospheric noise (Ferretti and others, 2001). Subsidence has been measured in a variety of urban settings with PSInSAR such as Mexico City and Bologna (Strozzi and others, 2003), Paris (Le Mouelic and others, 2002), and Pasadena (Werner and others, 2003). The PSInSAR technique has also been successfully applied to natural landscapes to detect motion of landslides (Colesanti and others, 2003b; Hilley and others, 2004), tectonics (Burgmann and others, 2006), and volcanoes (Lu and others, 2003; Hooper and others, 2004).

## Data Set

The synthetic aperture radar (SAR) data used in this study were acquired by the European Space Agency's (ESA) ERS-1, ERS-2 and ENVISAT satellites. The location of the 100 x 100 km frame is shown in figure 1. A time series of 41 scenes from 1993 to 2007 is used in the study (table 1). The available scenes for this area were selected from the data set maintained by ESA. The three SAR satellites have a 35-day repeat cycle but data are only collected for locations that have been previously requested by users. Therefore, the master data set from which these dates were chosen has gaps in the temporal coverage for this area. The acquisition dates were selected to 1) maximize the time span, 2) provide consistent coverage, and 3) give preference to non-growing season conditions where possible. It was found in a previous study that the Escalante Valley maintains more stable radar scattering properties during the winter months (Forster, 2006).

Using traditional InSAR processing, the 41 SAR scenes can theoretically be paired with each other to yield over 800 different interferometric pairs, each producing an interferogram or fringe image. However, using the PSInSAR technique one date is selected as the *master* and paired with each remaining scene producing 40 interferograms.

## PROCESSING

### Traditional InSAR and Persistent Scatterer InSAR

The data processing was done using programming modules from specialized SAR, InSAR, and PSInSAR software written by Gamma Remote Sensing. Customized Unix scripts were written to execute the Gamma commands required for this project.

The SARs onboard the ERS-1 and ERS-2 satellites are identical, with ERS-2 serving as the replacement for ERS-1. Therefore, data from the two satellites can be used interchangeably to form interferograms. The SAR onboard ENVISAT (ASAR), the follow-on to ERS-2, has a slightly different center frequency, 5.331 GHz, compared to 5.300 GHz for ERS-1 and 2. ASAR data can be used with ERS-1 and 2 for interferometry but requires additional processing steps that are done at the end of the processing stream. Since only 9 of the 41 scenes are ENVISAT, the initial processing steps described below were done with only the 32 ERS-1 and 2 scenes.

One SAR scene was first processed to a single-look-complex (SLC) image at the full spatial extent of the frame in order to select a subset boundary encompassing only

the Escalante Valley. This boundary was used to process all 32 scenes to SLCs, thus greatly reducing the processing time and disk storage required for the full scenes. The SLC is an image where each 8 x 4 m pixel is represented by an amplitude and phase of the returned radar pulse (backscatter). The master scene was then chosen based on 1) a Doppler centroid close to the mean Doppler centroid of all scenes, 2) minimizing the spatial baselines for the pairs, 3) low atmospheric distortion, and 4) acquisition

date near middle of data set time span. Using these hierarchical criteria (Gamma Remote Sensing, 2007) the scene acquired on 02/06/1996 was chosen for the master.

The other 31 SLC subsets (slaves) were then coregistered to the master subset. Detailed satellite position is required for this step and for the eventual computation of the spatial baselines; therefore, enhanced orbital tracking data were downloaded from the University of Delft,

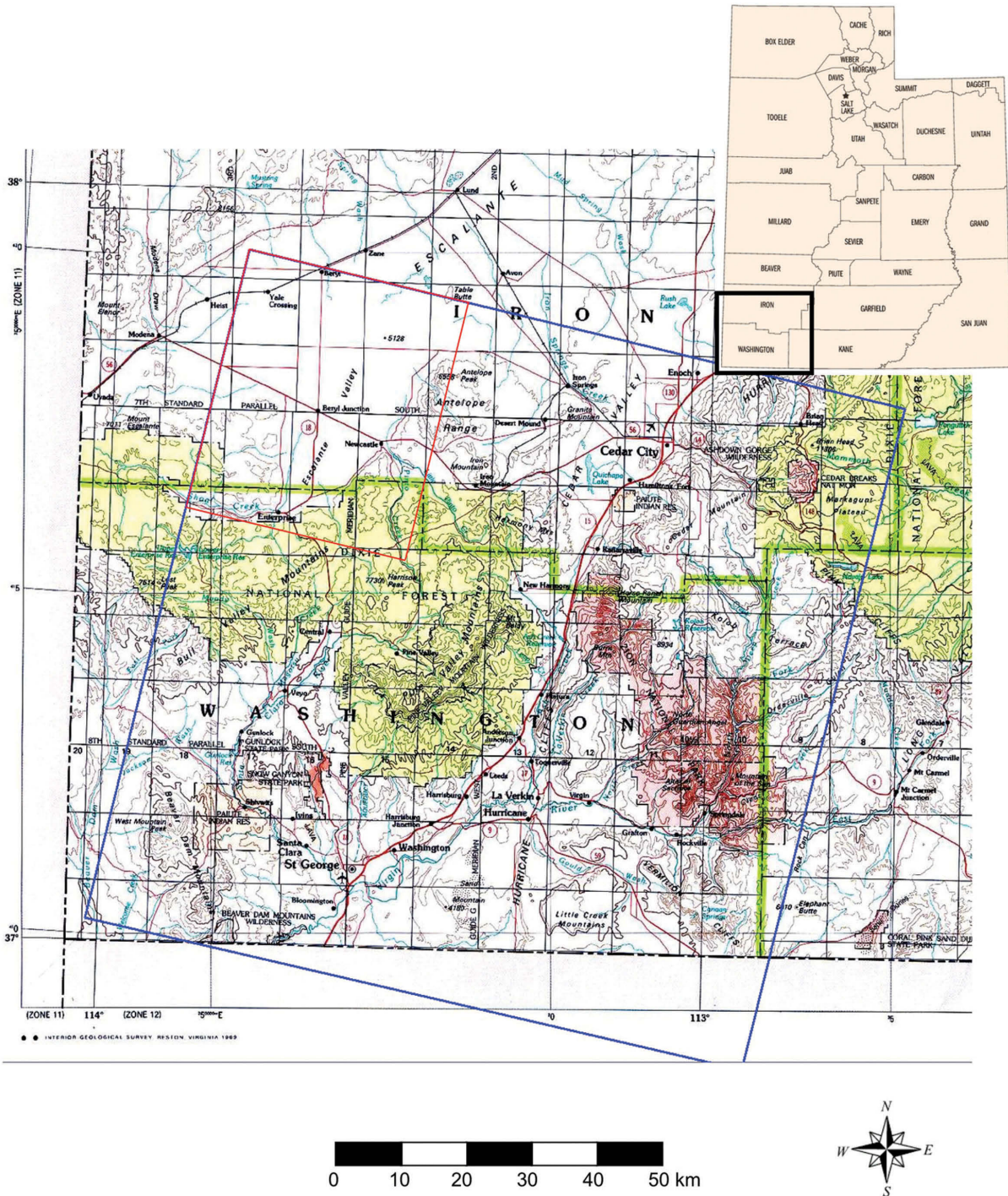


**Figure 1.** Southwest corner of Utah with blue box indicating approximate location of the SAR frame listed in table 1 and red box locating subsets used for interferograms in table 2 and figures 13 and 14. Inset map: <http://gazetteer.hometownlocator.com>; base map: U.S. Geological Survey, Reston, VA, 1989.

**Table 1.** Synthetic aperture radar (SAR) data used in this study. All scenes are frame number 2853.

Acquisition date	Satellite	Orbit
02/27/1993	ERS-1	8744
06/12/1993	ERS-1	9977
08/21/1993	ERS-1	10979
10/30/1993	ERS-1	11981
12/04/1993	ERS-1	12482
06/05/1995	ERS-1	20341
09/19/1995	ERS-2	2171
10/23/1995	ERS-1	22345
10/24/1995	ERS-2	2672
11/27/1995	ERS-1	22846
02/05/1996	ERS-1	23848
02/06/1996	ERS-2	4175
05/21/1996	ERS-2	5678
12/17/1996	ERS-2	8684
06/10/1997	ERS-2	11189
07/15/1997	ERS-2	11690
08/19/1997	ERS-2	12191
03/17/1998	ERS-2	15197
04/21/1998	ERS-2	15698
09/28/1999	ERS-2	23213
11/02/1999	ERS-2	23714
04/25/2000	ERS-2	26219
05/30/2000	ERS-2	26720
08/08/2000	ERS-2	27722
09/12/2000	ERS-2	28223
10/17/2000	ERS-2	28724
11/21/2000	ERS-2	29225
12/26/2000	ERS-2	29726
01/15/2002	ERS-2	35237
02/19/2002	ERS-2	35738
03/26/2002	ERS-2	36239
04/30/2002	ERS-2	36740
10/26/2004	ENVISAT	13894
11/30/2004	ENVISAT	14395
10/11/2005	ENVISAT	18904
11/15/2005	ENVISAT	19405
12/20/2005	ENVISAT	19906
05/09/2006	ENVISAT	21910
06/13/2006	ENVISAT	22411
12/05/2006	ENVISAT	24916
02/13/2007	ENVISAT	25918

The Netherlands, website for each scene. The master and 31 SLC slaves were initially coregistered to each other with pixel-scale offset. More precise offsets were determined using correlation matching to 1/10th of a pixel. Each slave SLC was coregistered to the master SLC and resampled. The phase for each pixel of the master was subtracted from the resealed phase of the slave to form an interferogram for all 31 pairs. Coherence images for each pair were also formed, representing the local spatial homogeneity of the phase in the interferogram. Areas of high coherence have a reliable phase signal and the phase can be used to calculate surface displacement, whereas areas of low coherence have a noisy phase signal and were not included in displacement maps.

### Persistent Scatterer InSAR

The processing steps described above are the same for traditional InSAR and PSInSAR. The remainder of this section will describe additional steps used for the PSInSAR processing. Candidate pixels containing persistent scatterers (PS) need to be identified. A persistent scatterer is an object or group of objects within a single pixel that returns the radar signal in a consistent manner over the time span of the data set and also over small changes in the viewing geometry of the radar-look orientation (Ferretti and others, 2001). A typical example of persistent scatterers are sides of buildings along streets where the perpendicular structure of the building wall relative to the street creates a double-bounce reflection of the radar signal back to the side-looking satellite (Colesanti and others, 2003a). More subtle objects such as individual fence posts and power-line and telephone poles have been identified as PS (Dehls, 2005). Natural features like rock outcrops and desert pavement have also been used as PS (Hooper and others, 2004).

There are two general characteristics that can be used to identify pixels dominated by persistent scatterers. The first is temporal stability. A PS will return the same intensity in each SAR scene over time even though the slight variations in the orbits alter the viewing geometry of the scenes. Therefore, candidate pixels are those that have a more consistent return intensity compared with the average variability of intensity for all pixels in the scene over the time span of the data set. The second characteristic, spectral stability, that distinguishes PS is not based on a time series but can be identified from a single SAR scene. PS will have a stable return even if different bandwidths are used to process the same SAR scene. Candidate PS are identified using a combination of the temporal and spectral stability criteria.

## PSInSAR RESULTS

After numerous iterations of varying thresholds for temporal and spectral stability the most reliable set of PS was found for the Escalante Valley (figure 2). Candidate pixels dominated by PS are shown in yellow over a background geocoded SAR image. The background SAR image is the mean backscatter intensity of all 32 ERS SAR images and lacks clarity in some areas of the valley, as explained below. The density of PS in the valley is orders of magnitude less than typical applications of PSInSAR for subsidence mapping (Colesanti and others, 2003a).

The density of PS is important because, as with traditional InSAR, the phase of the returned signal is only measured within a single phase cycle between 0 and 360 degrees. The number of phase cycles for each pixel is unknown and the phase of the interferogram is said to be wrapped at this stage in the processing. Traditional InSAR processing assumes the land surface deforms uniformly for

adjacent pixels; therefore, the phase should vary only between 0 and 360 degrees for neighboring pixels. Consequently, if the phase value is assumed to be known at an arbitrary seed pixel surrounded by other pixels with a clean phase signal, the phase of the entire region can be determined in a relative sense. This is done by adding the phase changes of adjacent pixels and propagating outward from the seed pixel and effectively *unwrapping* a portion of the scene. The spatial extent of the unwrapping is determined by the area of contiguous pixels with reliable phase. PSInSAR relaxes the restriction on requiring contiguous pixels with a good phase signal by identifying isolated PS pixels, which by definition should have a reliable phase (figure 2). However, the PS pixels must also be unwrapped. Since they are not contiguous, as in traditional InSAR, additional information and an assumption are required to unwrap the PS. The assumption is that the ground deformation varies in a predictable manner with respect to time, usually linearly. The additional information is the time history of the PS phase available from the

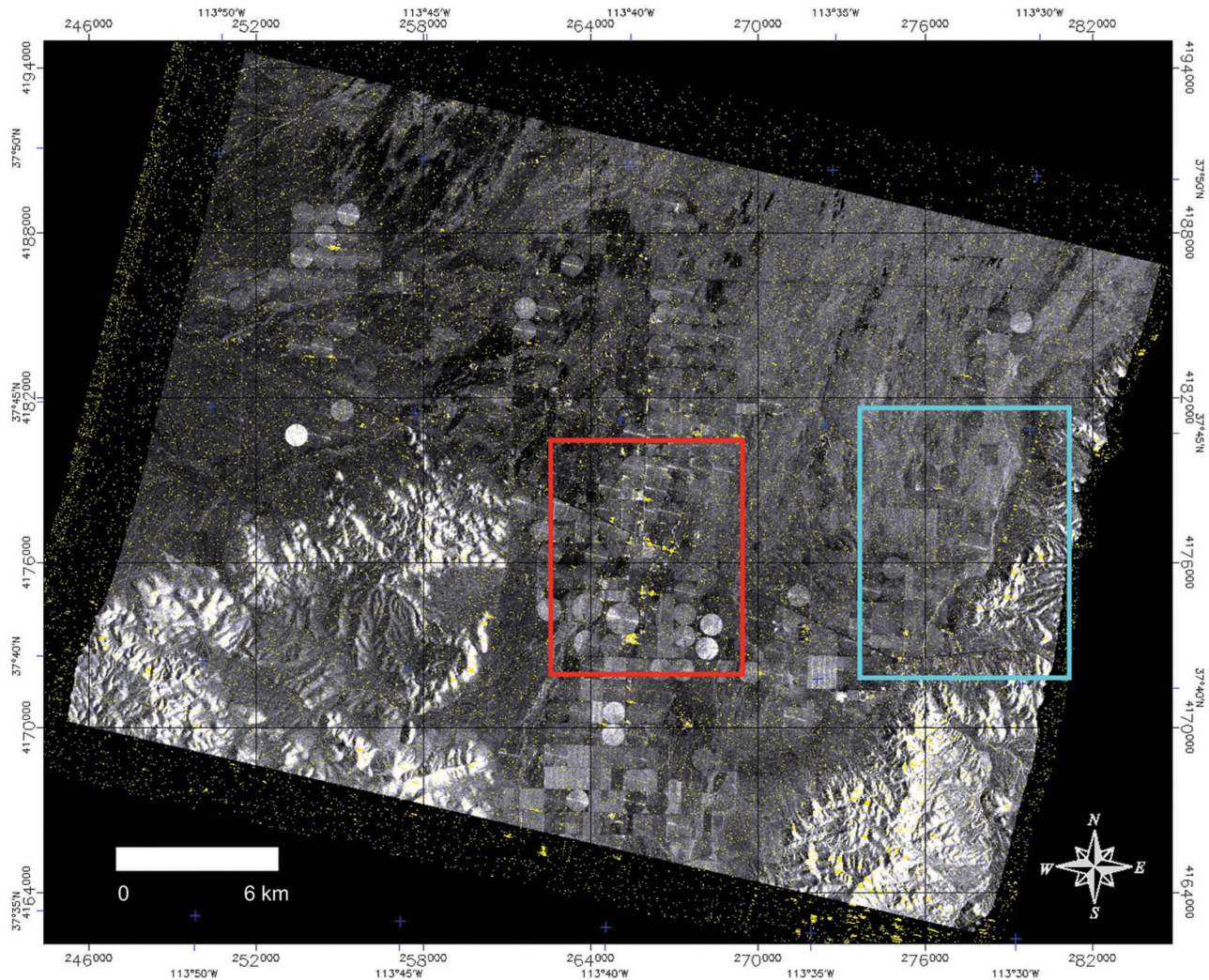


**Figure 2.** SAR image of Escalante Valley, Utah, representing mean backscatter for 32 ERS-1/2 scenes (table 1.) Yellow dots are candidate persistent scatterers based on optimal spectral and temporal stability thresholds. Red box is the location of figures 3, 4, and 5. Blue box is location of figure 10.

series of multiple SAR images, in this case 32 ERS scenes from 1993–2002 (Table 1). PSInSAR requires a stack or time series of interferograms (typically >15) while traditional InSAR can operate on a single interferogram made from two SAR images (Ferretti and others 2001).

The low spatial density of the PS in figure 2 (131,256 points) causes problems unwrapping the phase. The time history of the phase for each of the PS is apparently not enough to compensate for the sparse number of PS in the Escalante Valley. An unwrapped PS interferogram after baseline and topographic effects have been removed is shown in figure 3a. The random color of neighboring PS indicates the phase has no spatial continuity and is therefore unwrapped incorrectly. Continued PSInSAR processing with these PS points resulted in unrealistic random land deformation over time at these locations.

The number of candidate PS in the Escalante Valley was increased in an effort to avoid the unwrapping errors due to low point-density. The threshold for temporal stability used to define candidate PS was lowered and resulted in nearly an order of magnitude increase to a total of 913,918

PS points (figure 4). After unwrapping, a similar pattern of random phase is also present in this PS interferogram (figure 3b). The increase in candidate PS density is offset by the decrease in the reliability of the added points. The threshold for spectral stability used to define candidate PS was also lowered and resulted in increased candidate PS, but the same types of unwrapping errors and unrealistic time series of deformation were also found. Additional iterations involving changes to both temporal and spectral stability thresholds did not give more encouraging unwrapping results or realistic deformation models. It is therefore concluded the spatial density of PS in the Escalante Valley is insufficient to use the PSInSAR technique to map land deformation. This prompted an investigation of the features responsible for the candidate PS in the Escalante Valley.

### INVESTIGATION OF PS LOCATIONS

Selected PS locations were identified on Digital Orthorectified Quadrangle (DOQ) aerial photographs and visited

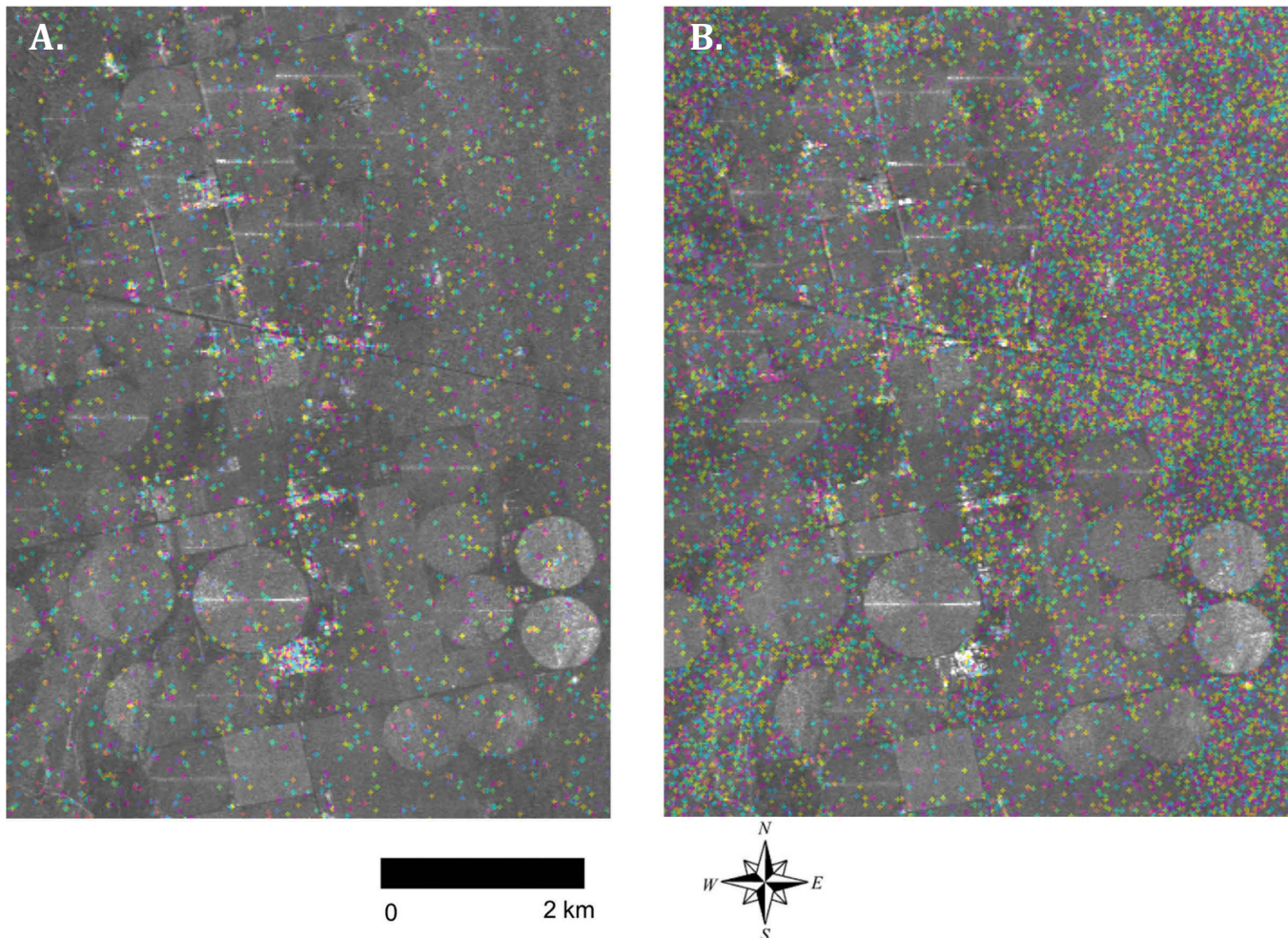


**Figure 3.** Phase of candidate persistent scatterers shown with color over SAR image of Escalante Valley, Utah representing mean backscatter for 32 ERS-1/2 scenes (table 1). Candidate persistent scatterers based on a) optimal spectral and temporal stability thresholds and b) relaxed threshold values. Location shown in figures 2 and 4.

in the field on 6/19/2007. The most recent DOQs available for download from the Utah Automated Geographic Reference Center (AGRC) were acquired in 1983. Figure 5a shows the position of PS in the vicinity of Beryl Junction. Three of the large sets of PS clusters are identified on a portion of the DOQ (q3705\_83, figure 5b). There are obvious structures and groups of structures associated with PS clusters 1 through 5, but elsewhere more extensive groups of structures were not identified as PS clusters (figure 5).

The northern part of this area was examined in more detail (figure 6). The PS 1 cluster is a set of two sheet metal two-story buildings surrounded by gravel/bare ground (labeled 1 in figure 7). Directly across the road west of PS 1 is a dairy farm consisting of many one-story buildings and feed lots, occupying a quarter of a circular field (labeled A in figure 7). Only a few PS are associated with this farm (site A, figure 6) compared to the large

cluster of PS for the two buildings across the street (PS cluster 1, figure 6). The structure at the SW corner of the circular field south of PS cluster 1 (labeled B in figures 6b and 7) has a metal roof with no sides, and is surrounded by vegetation-covered ground. Only two PS pixels are associated with this structure (figure 6a). Across the road to the west, a set of buildings is mostly surrounded by trees serving as a windbreak (labeled C in figures 6b and 7) and accounts for a few isolated PS (figure 6a). The large linear cluster of PS 2-5 (Fig 6) is from a series of buildings lining both sides of state route 56 east of the intersection with route 18 (figure 8).

The southern portion of figure 5 is dominated by the large PS cluster 6. Details of this processing facility are shown in figure 9. There are several metal buildings and large areas of gravel/bare ground within and surrounding the facility. The number of buildings has increased since the DOQ was acquired in 1983.

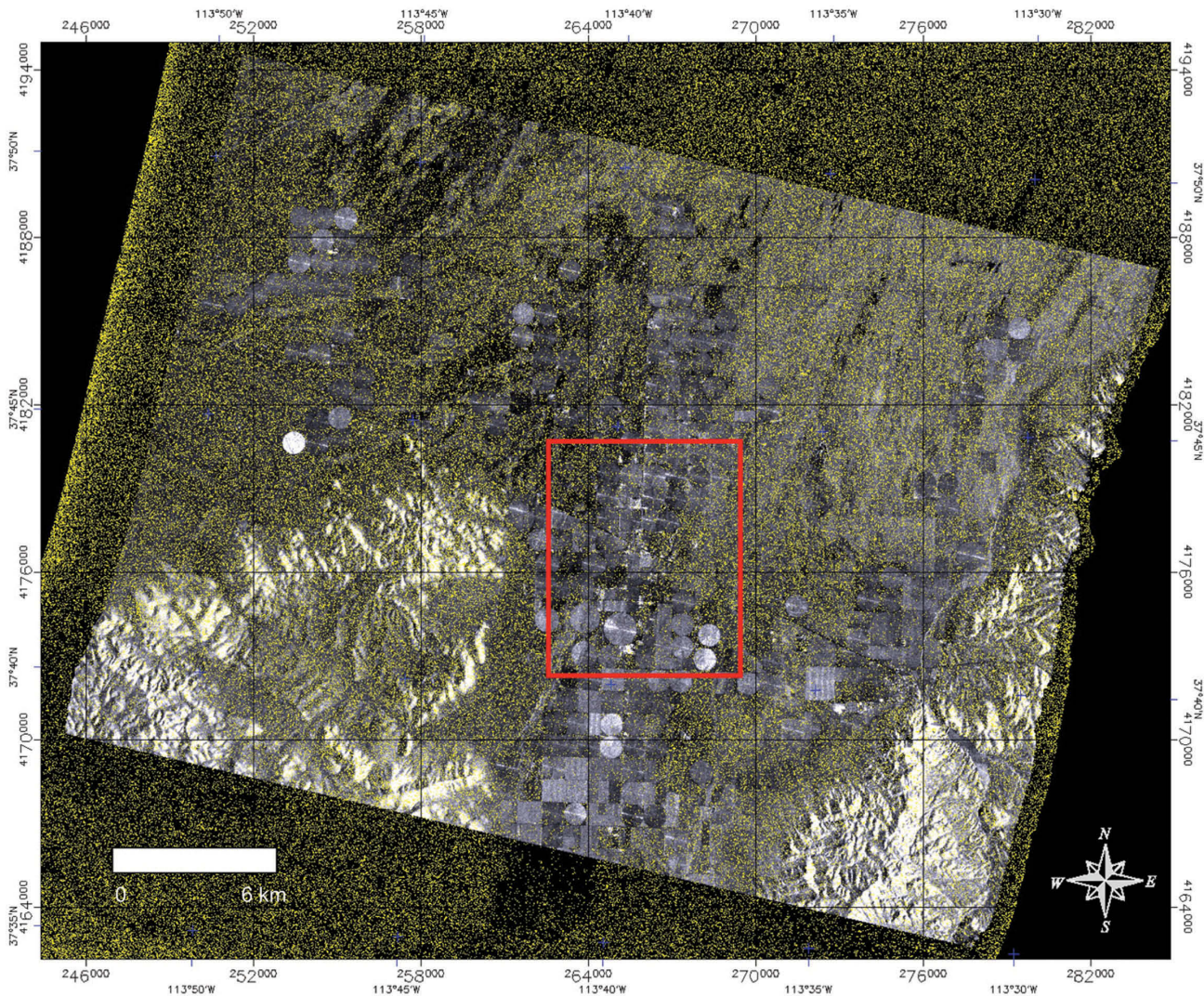


**Figure 4.** SAR image of Escalante Valley, Utah, representing mean backscatter for 32 ERS-1/2 scenes (table 1.) Yellow dots are candidate persistent scatterers based on relaxed threshold values of spectral and temporal stability. Red box is the location of figure 3b.

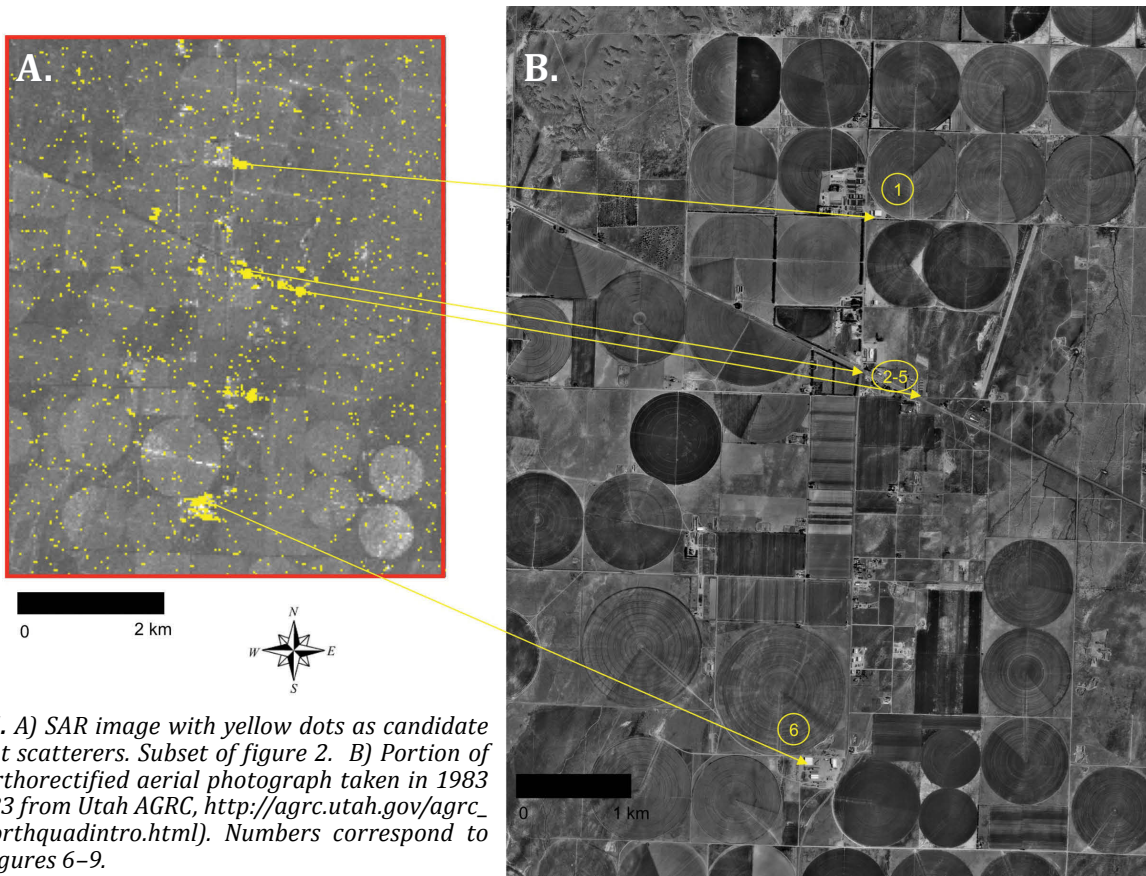


**Figure 5.** A) SAR image with yellow dots as candidate persistent scatterers. Subset of figure 2. B) Portion of digital orthorectified aerial photograph taken in 1983 (q3705\_83 from Utah AGRC, [http://agrc.utah.gov/agrc\\_sgid/digorthquadintro.html](http://agrc.utah.gov/agrc_sgid/digorthquadintro.html)). Numbers correspond to sites in figures 6–9.

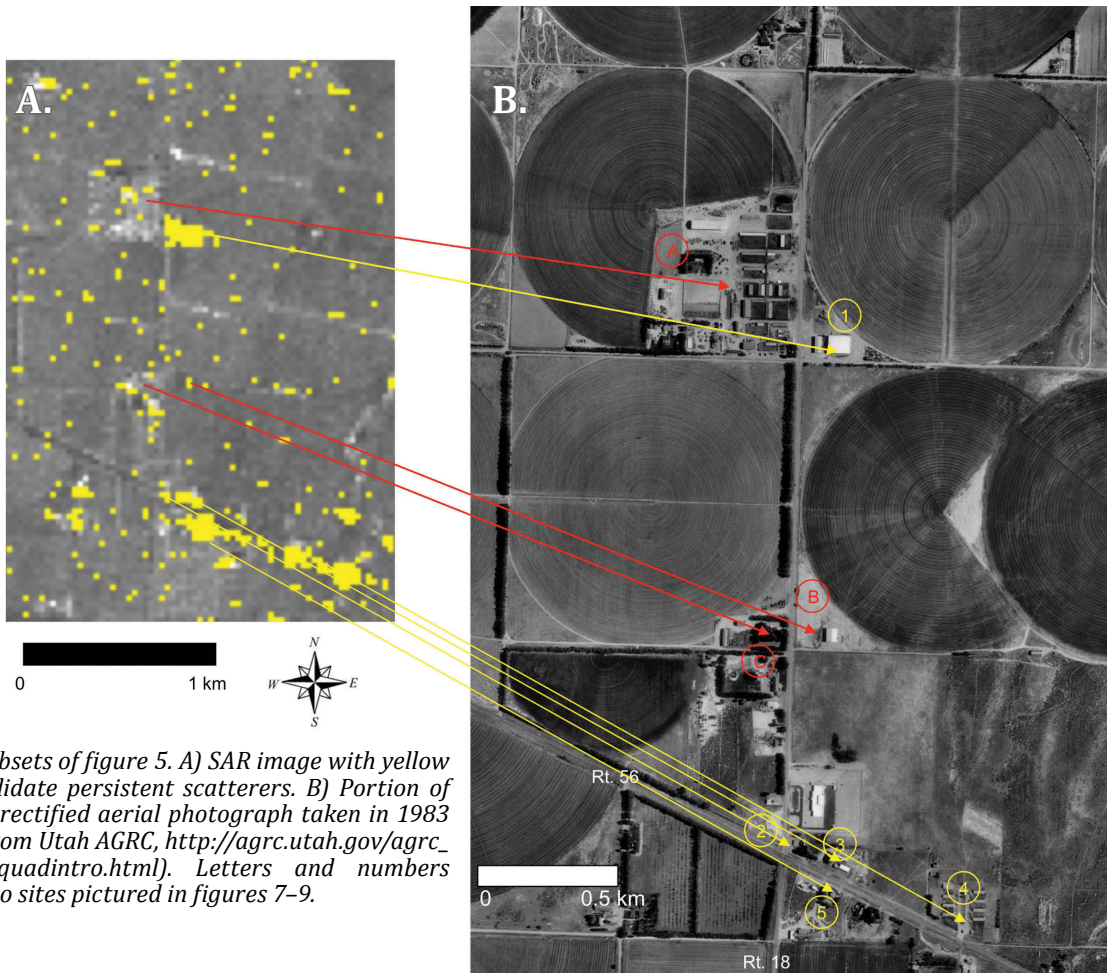


**Figure 6.** Subsets of figure 5. A) SAR image with yellow dots as candidate persistent scatterers. B) Portion of digital orthorectified aerial photograph taken in 1983 (q3705\_83 from Utah AGRC, [http://agrc.utah.gov/agrc\\_sgid/digorthquadintro.html](http://agrc.utah.gov/agrc_sgid/digorthquadintro.html)). Letters and numbers correspond to sites pictured in figures 7–9.



Figure 7. Photographs of features north of Beryl Junction labeled in figure 6 taken on 6/19/2007.



Figure 8. Photographs of persistent scatterer clusters at Beryl Junction labeled in figure 6 taken on 6/19/2007.



**Figure 9.** Photographs of a persistent scatterer cluster south of Beryl Junction labeled in figure 5 taken on 6/19/2007.

Another area of notable PS pattern is along the eastern-most edge of the Escalante Valley just north of Newcastle (blue box in figure 2). Details of the SW-NE trending line of PS are shown in figure 10. The corresponding area on the DOQ (q3706\_83) indicates the line of PS is associated with a set of high-tension power lines (figure 10c). The field photograph taken on the north side of Utah Route 56 near Newcastle shows the metal towers used to support the power lines (figure 10a). Single wooden electrical poles lining Route 56 and crossing other portions of the Escalante Valley did not qualify as PS (figure 11).

Other structures in the valley did not classify as PS (figure 11). Many of the houses are surrounded by trees and vegetation and were not classified as PS. Some of the houses and farm buildings appear relatively new and were probably constructed during the SAR time series. An example of one large building that is not classified as PS and appears to have been constructed in the last 10 years is the school at Beryl Junction (figure 11).

Changes in the agricultural field shapes during the SAR time series, observable in the SAR images, will also

reduce the number of PS. As mentioned above, the average of all 32 ERS SAR scenes is used as background in figure 2 because it minimizes the unwanted speckle, or pixel-to-pixel scale variation of intensity, that can make SAR images appear noisy. However, if there are significant changes in the backscatter over time due to real changes in the land cover, the average image will lose detail in those areas. This appears to be the case for the agricultural areas of the Escalante Valley. A selection of the SAR images for three winter dates (2/27/1993, 12/26/2000, and 2/19/2002) indicates backscatter changes (from growing crops) and changes in the geometry of a given field over time (figure 12). Several of the rectangular fields have been progressively converted to circular pivot irrigation fields from 1993 to 2002. This was verified on the ground where a series of rectangular fields, shown in the 1983 DOQ and a 1993 SAR image, is now a circular field.

The field observations and the aerial photographs of PS locations and features not classified as PS leads to some general conclusions about the viability of using the PSInSAR technique to map land deformation in the

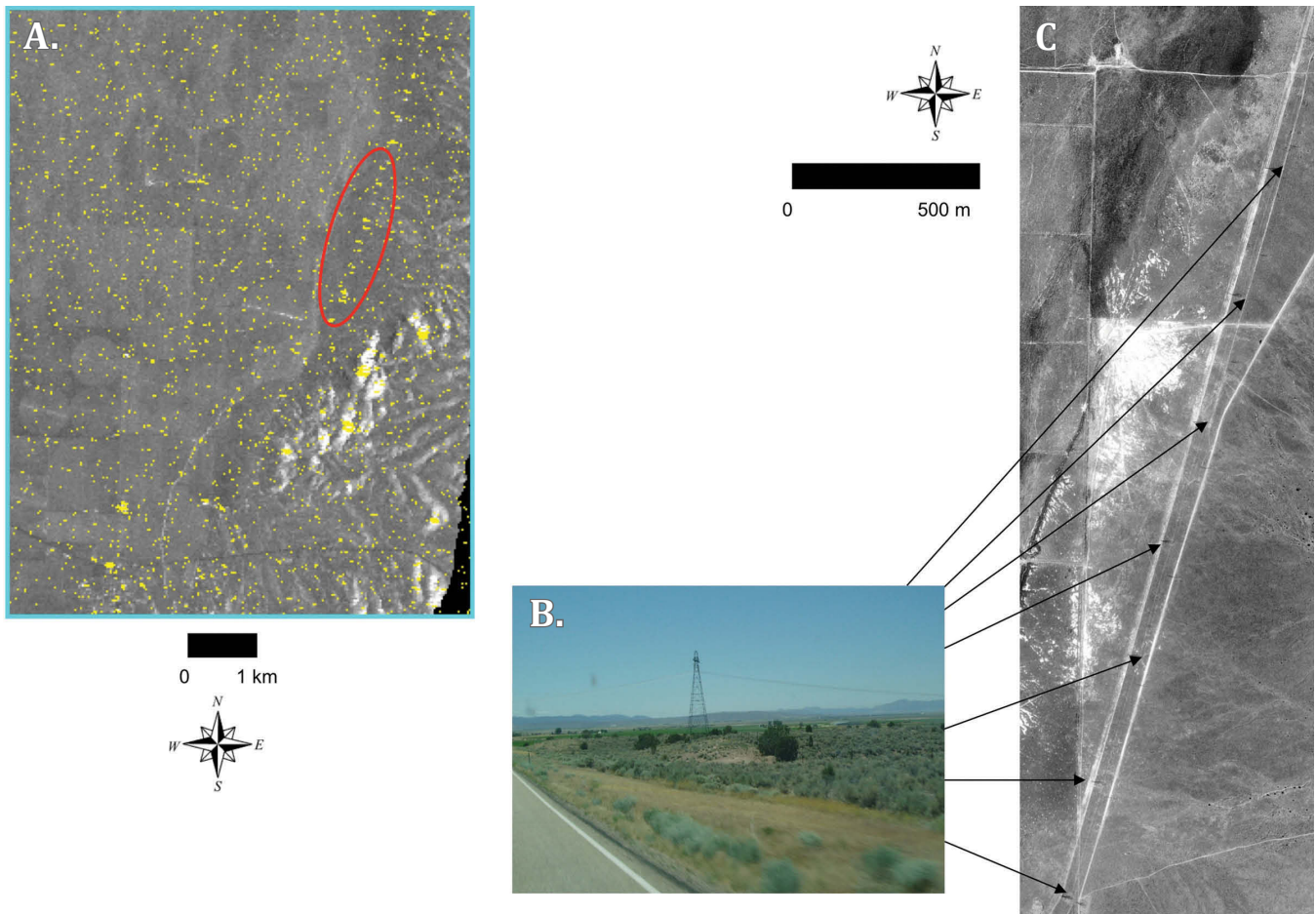


**Figure 10.** Power lines northeast of Newcastle. A) Candidate persistent scatterers over a SAR image subset of figure 2. Red ellipse is the area of 10c. B) Photograph of a metal power line tower. C) Metal power line towers on a portion of digital orthorectified aerial photograph taken in 1983 (q3706\_83 from Utah AGRC, [http://agrc.utah.gov/agrc\\_sgld/digorthquadintro.html](http://agrc.utah.gov/agrc_sgld/digorthquadintro.html)).



**Figure 11.** Photographs of features that were not classified as candidate persistent scatterer clusters in the Escalante Valley taken on 6/19/2007.

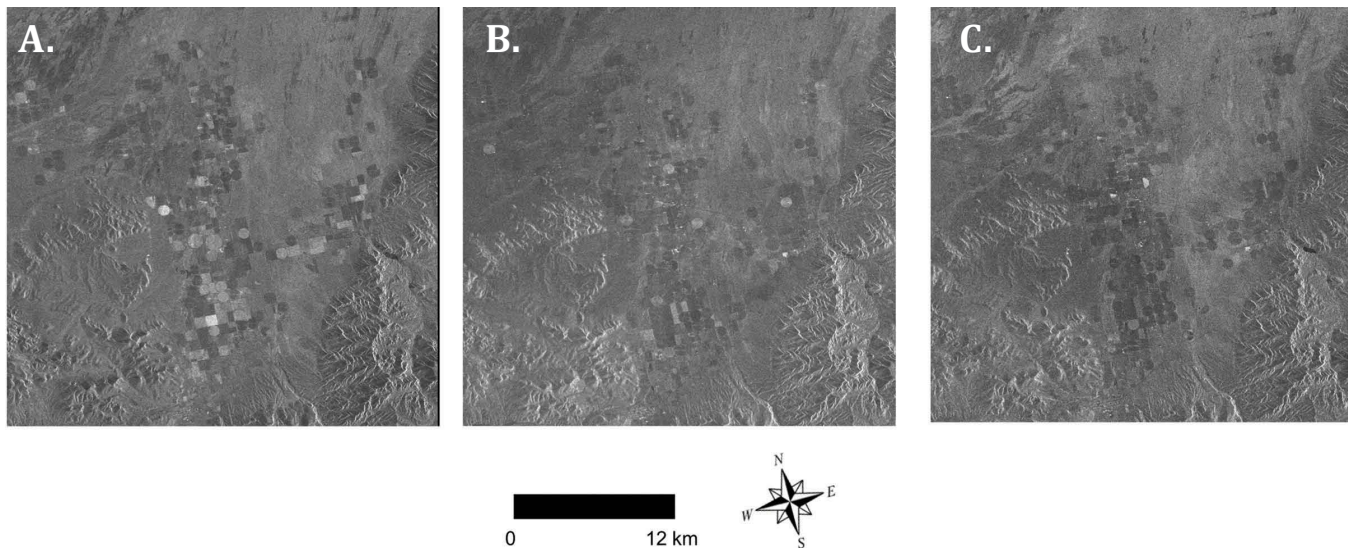


**Figure 12.** Series of SAR images of the Escalante Valley acquired on A) 2/27/1993, B) 12/26/2000, C) 2/19/2002.

Escalante Valley. Buildings surrounded by gravel/bare ground are more likely to be PS than similar size structures with trees or vegetation adjacent to the building. The bare ground is a stable and strong spectral reflector of the radar signal directing it forward to the side of the building where it can reflect back to the radar via a double-bounce geometry. Vegetation is a more diffuse scatterer and less temporally stable, thereby decreasing the probability of getting a temporally or spectrally stable double-bounce return. Multi-story buildings, which present a larger double-bounce target, are more likely to be PS than single story buildings. Covered structures without sides are less likely to produce PS. Metal power line towers are conductive and large enough to qualify as PS while the smaller and less conductive wooden poles are not. There are not enough quality PS in the Escalante Valley to use the PSInSAR technique.

## RECENT DEFORMATION MAPS FROM TRADITIONAL INSAR

The long-time series of SAR scenes (table 1) also provides the opportunity to produce displacement maps using traditional InSAR techniques. A previous study mapped the subsidence of the Escalante Valley from 1993 to 1998 (Forster, 2006). The deformation from 1998 to 2006 will be the focus of the remainder of this report.

### Phase unwrapping procedure

Interferograms from all combinations of ERS-2 and ASAR scenes that presented reasonable baselines (< 500m) and time spans of interest were processed. The goal was to determine if changes occurred in the spatial patterns or magnitude of the subsidence in the Escalante Valley over

**Table 2.** Interferometric pairs used to make displacement maps.

Acquisition dates	Elapsed time (days)	Baseline (m)
04/21/1998–11/02/1999	560	80
11/02/1999–10/17/2000	350	250
10/26/2004–11/15/2005	385	146
10/11/2005–12/05/2006	420	306

the time period 1998 to 2006. Since the coherence typically degrades as time between acquisitions increases, a set of annual displacement maps is the optimal sequence to observe change over this eight-year span. However, the acquisition dates available, baselines, atmospheric noise, and coherence limited the pairings and the best set of interferograms are listed in table 2.

The interferograms in table 2 were unwrapped and converted to displacement maps. The unwrapping technique used is different from the branch-cut method applied in the previous InSAR study of subsidence in Escalante Valley (Forster, 2006). The branch-cut method (Goldstein and others, 1988) can only unwrap pixels that are contiguous to the seed pixel, which is selected as the starting point for phase unwrapping. Therefore, if there is even a one-pixel gap in good coherence the phase unwrapping will not proceed any further. In the Escalante Valley this can be spatially limiting because changing agricultural fields segment the area. Therefore, this study used a minimum cost flow (MCF) unwrapping technique (Costantini, 1998). Prior to unwrapping the interferogram has the phase contributions from topography and baseline removed using a digital elevation model (DEM) and precision satellite orbit tracks. The interferogram is then filtered with a spatially adaptive filter to reduce the phase noise. An unwrapping validity mask is made

based on the coherence of the interferogram. All pixels with coherence less than 0.3 were masked out and not included in the subsequent unwrapping. The MCF procedure first generates a triangular mesh network of all unmasked pixels (Gamma Remote Sensing, 2007). This allows gaps in the interferogram to be bridged. The coherence of the unmasked pixels are used as weights giving more emphasis to those pixels with high coherence (low phase noise) and less emphasis to those pixels with low coherence (high phase noise). This allows the cost of phase discontinuities over the entire scene to be computed. MCF analyzes the cost of all flow paths through the scene and chooses the one with a minimal total cost (Costantini, 1998). This unwrapping technique minimizes global unwrapping errors and allows for disconnected areas to be unwrapped and incorporated into displacements maps. The unwrapped phase is converted to a relative displacement map by assuming the ground surface motion was all in the vertical direction. The relative displacement is transformed to absolute displacement by selecting an area of suspected stability, assigning that to zero displacement, and applying the offset to the remainder of the unwrapped pixels.

### Subsidence maps

The magnitude and pattern of subsidence over the period 1998 to 2006 is analyzed with a set of displacement maps derived from the four interferometric pairs in table 2. Figure 13a–d are vertical displacement maps with negative displacement representing subsidence. The color scale's upper range for each displacement map varies in order to present the most spatial detail in each map. Areas without color were not unwrapped because of low coherence or have no subsidence. The color is opaque to show features of the underlying gray-scale Landsat ETM+ near infrared band that highlights vegetation.

The vertical displacement from 4/21/1998 to 11/2/1999 (figure 13a) includes most of two growing seasons (summers of 1998 and 1999). The spatial pattern is similar to both the 1993 to 1996 and 1996 to 1998 InSAR displacement maps derived previously for the Escalante Valley (Forster, 2005). The fundamental difference is the increased spatial extent of the displacement measurement. This is due to the improved coherence from shorter temporal baseline and the MCF unwrapping processes allowing non-contiguous pixels to be unwrapped.

The displacement map for 11/2/1999 to 10/17/2000 (figure 13b) has a similar spatial extent but fewer gaps than figure 13a. This is probably due to the shorter time period between acquisitions. Most gaps in the displacement map are shown to be directly related to the circular pivot-irrigation fields as the shapes of the gaps are circular or formed by a series of contiguous circles. The location of water wells and the contours of change in ground-

water level from 1949 to 2002 (Lund and others, 2005) are also shown in figure 13b. Some of the areas of higher subsidence (red circles) are associated with water wells while other areas with wells (blue circles) have minimal subsidence (figure 13b). The pattern of groundwater change contours does not appear to be similar to the displacements. The location of earth fissures observed by the UGS during the winter 2004/2005 (Lund and others, 2005) are also shown on figure 13b, and the northern fissures are associated with larger displacements. Displacement maps for the next two time periods (10/26/2004 to 11/15/2005 and 10/11/2005 to 12/5/2006) (figure 13c and d) have similar patterns to the previous two (figure 13a and b).

To observe recent trends in subsidence and assess the differences between the four time periods subsidence rate maps are analyzed (figure 14a–d). The negative vertical displacement is divided by the number of days between acquisition pairs then converted to a subsidence rate in centimeters per year. The same color scale is used for each map and the opacity of the color is removed so that the texture of the underlying near-infrared image no longer modulates the color (as it does in figure 13).

The general pattern of subsidence in the Escalante Valley is consistent from 1998 to 2006; however the magnitude of subsidence has increased in local areas (figure 14). The overall pattern consists of two main subsidence lobes, a northeastern arm and a northwestern arm, separated by a NNE-SSW trending ridge of reduced subsidence. Subsidence rates in the northern centers of both lobes increased from approximately 3 cm/yr. to near 6 cm/yr. from 1998–1999 (figure 14a) to 1999–2000 (figure 14b). The remainder of the valley maintained consistent subsidence rates between 1.5 and 3.0 cm/yr. The next subsidence rate map (2004–2005, figure 14c) shows a new center of maximum subsidence within the NW lobe, farther north and west of the previous area of maximum subsidence (figure 14b). The other notable change is the increasing subsidence rate just west of the ridge separating the two lobes. This zone of increased subsidence rate parallels the ridge southward to near the southern end of the measurable displacement (37°38'N, figures 14c and 14d). The final subsidence rate map (2005–2006, figure 14d) indicates a contraction of this linear subsidence feature leaving two zones of high subsidence rate at the northern and southern ends of the previous feature. There is also an apparent expansion of the subsidence rate maximum in the NW lobe indicated by an increased area of red (near 6 cm/yr.).

Changes in subsidence rate are analyzed by subtracting figure 14b from figure 14d, providing a change in subsidence rate from the time period of 11/2/1999 to 10/17/2000 with 10/11/2005 to 12/5/2006 (figure 15a). The earliest time period (4/21/1998 to 11/2/199, figure

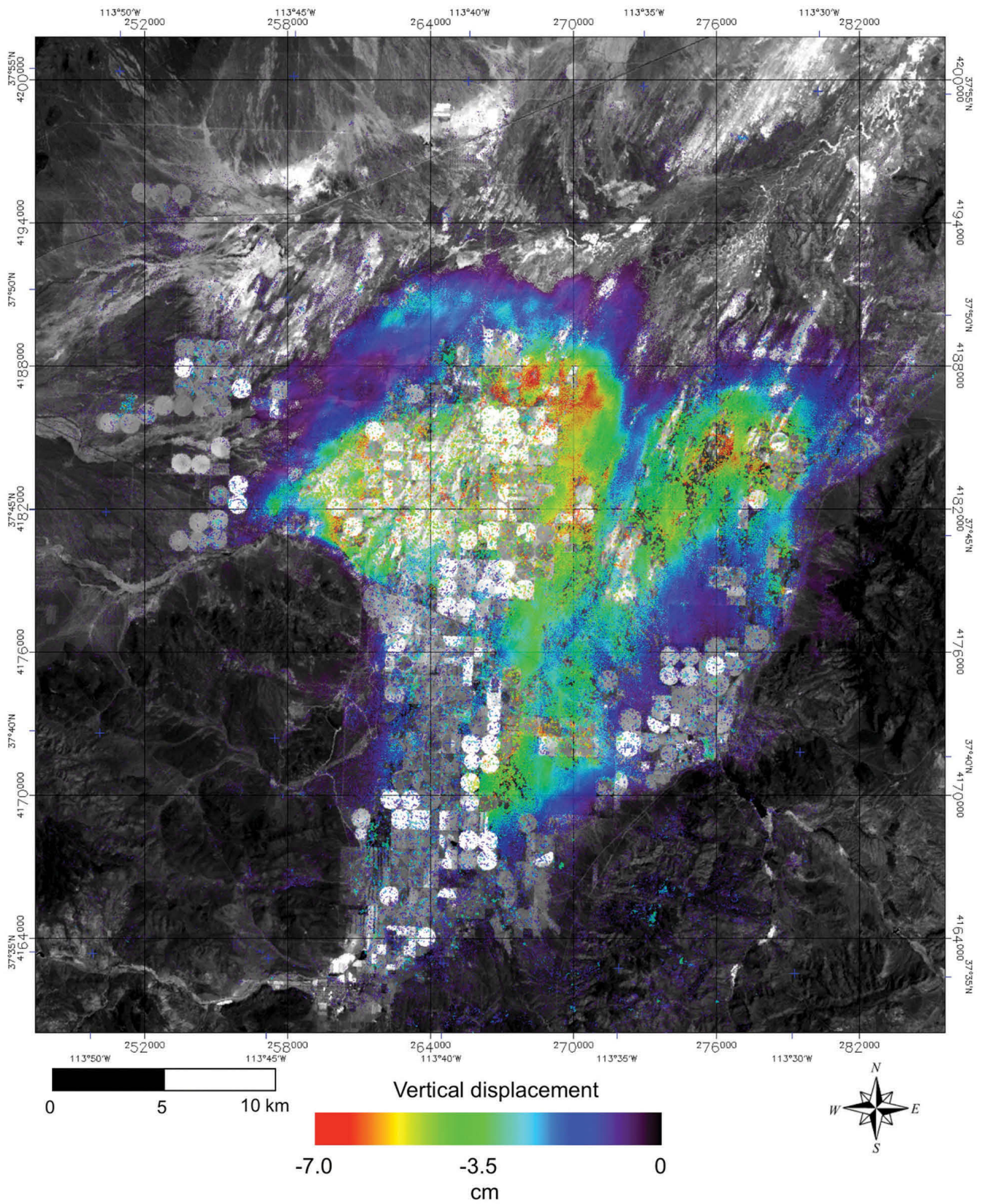


**Figure 13a.** Vertical displacement map of the Escalante Valley from InSAR pair 4/21/1998–11/2/1999 as opaque color over Landsat ETM+ band 4 in gray-scale. Negative values indicate surface lowering relative to bedrock. Color is the extent of the usable data.

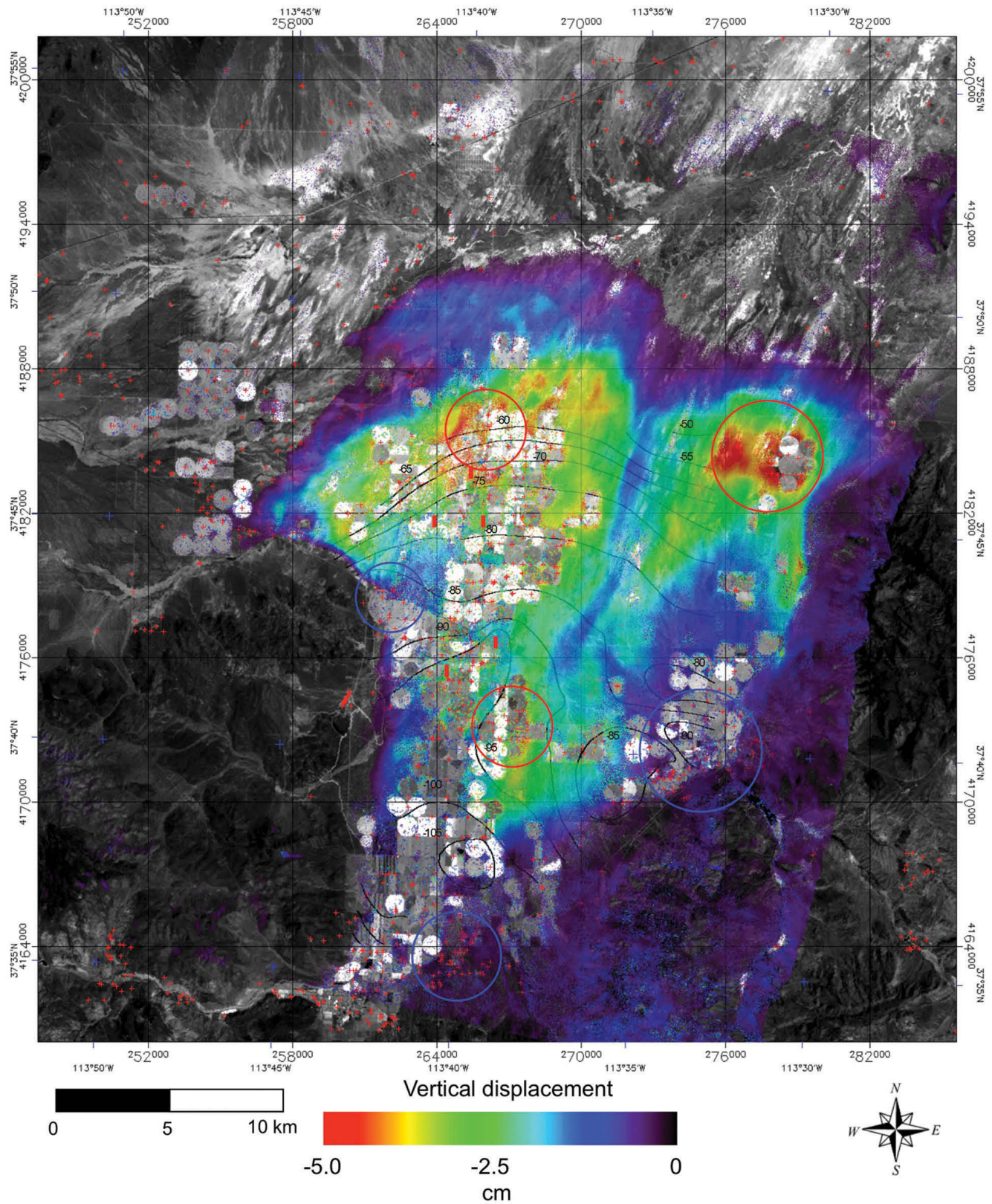


**Figure 13b.** Vertical displacement map of the Escalante Valley from InSAR pair 11/2/1999–10/17/2000 as opaque color over Landsat ETM+ band 4 in gray-scale. The location of water wells are shown as red crosses. Red rectangles show locations of earth fissures (Lund and others, 2005). The contours are of change in groundwater level (in feet) from 1949 to 2002 (Lund and others, 2005). Circles are clusters of water wells associated with areas of higher (red) and minimal (blue) subsidence.

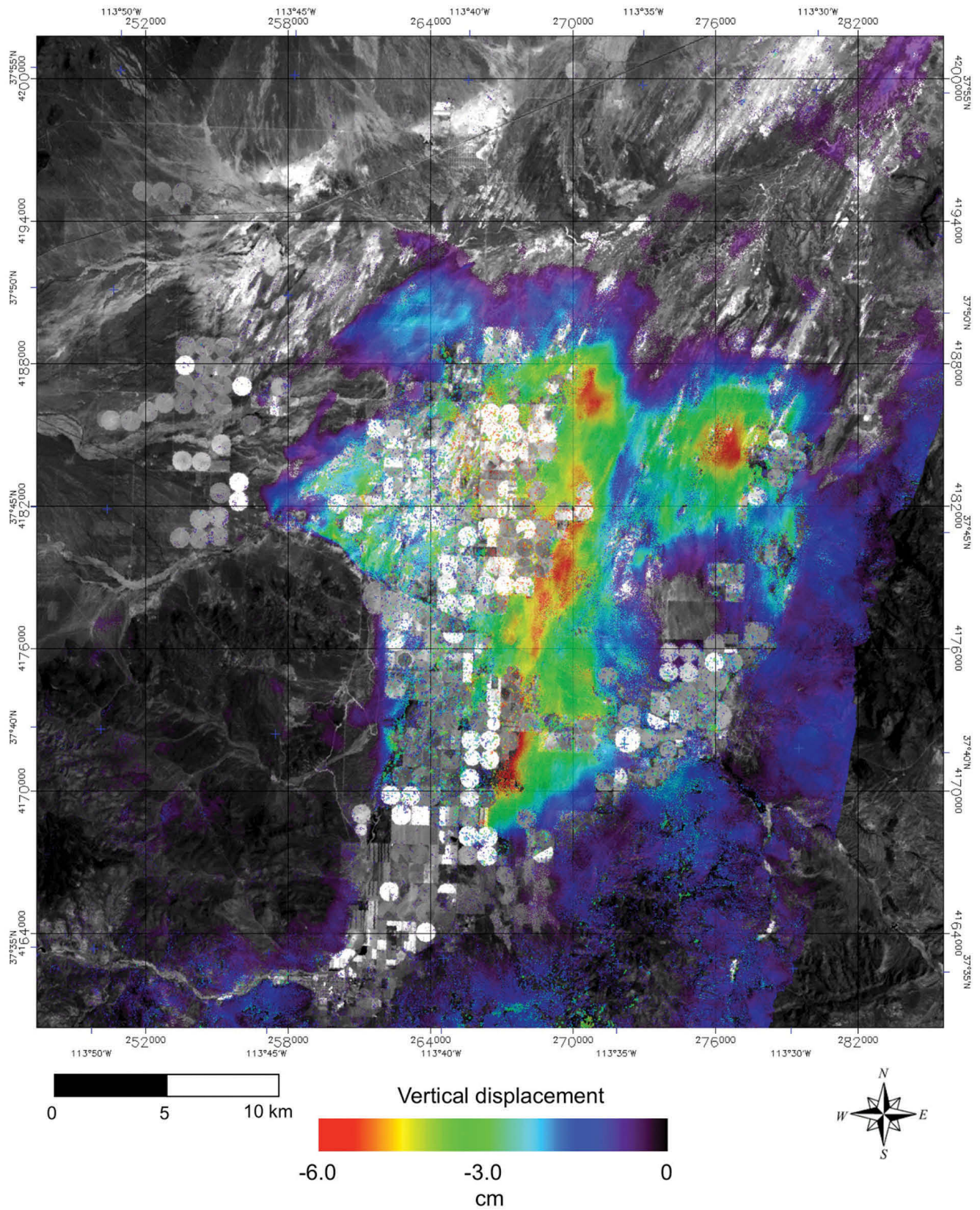


**Figure 13c.** Vertical displacement map of the Escalante Valley from InSAR pair 10/26/2004–11/15/2005 as opaque color over Landsat ETM+ band 4 in gray-scale. Negative values indicate surface lowering relative to bedrock. Color is the extent of the usable data.

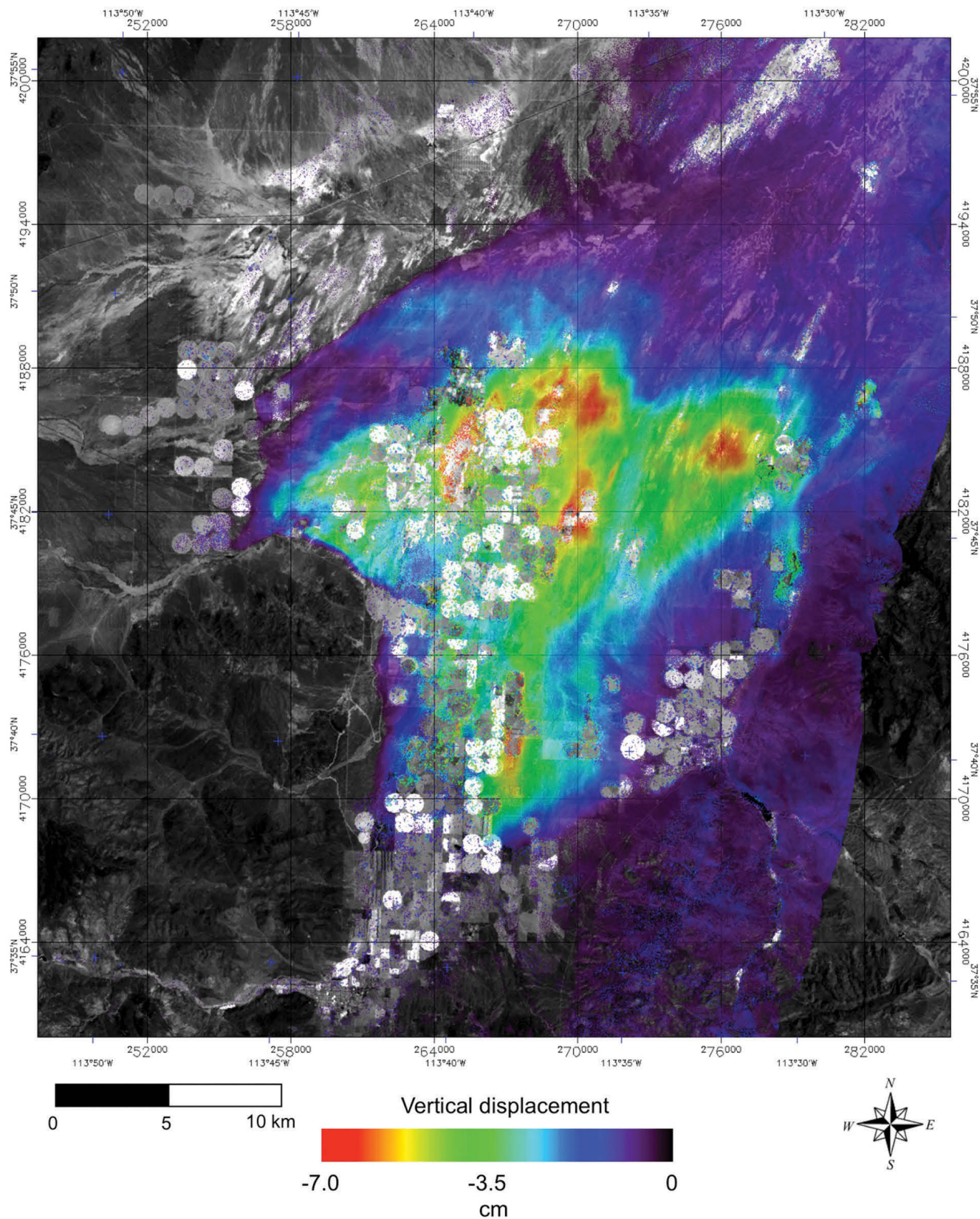


**Figure 13d.** Vertical displacement map of the Escalante Valley from InSAR pair 10/11/2005–12/5/2006 as opaque color over Landsat ETM+ band 4 in gray-scale. Negative values indicate surface lowering relative to bedrock. Color is the extent of the usable data.

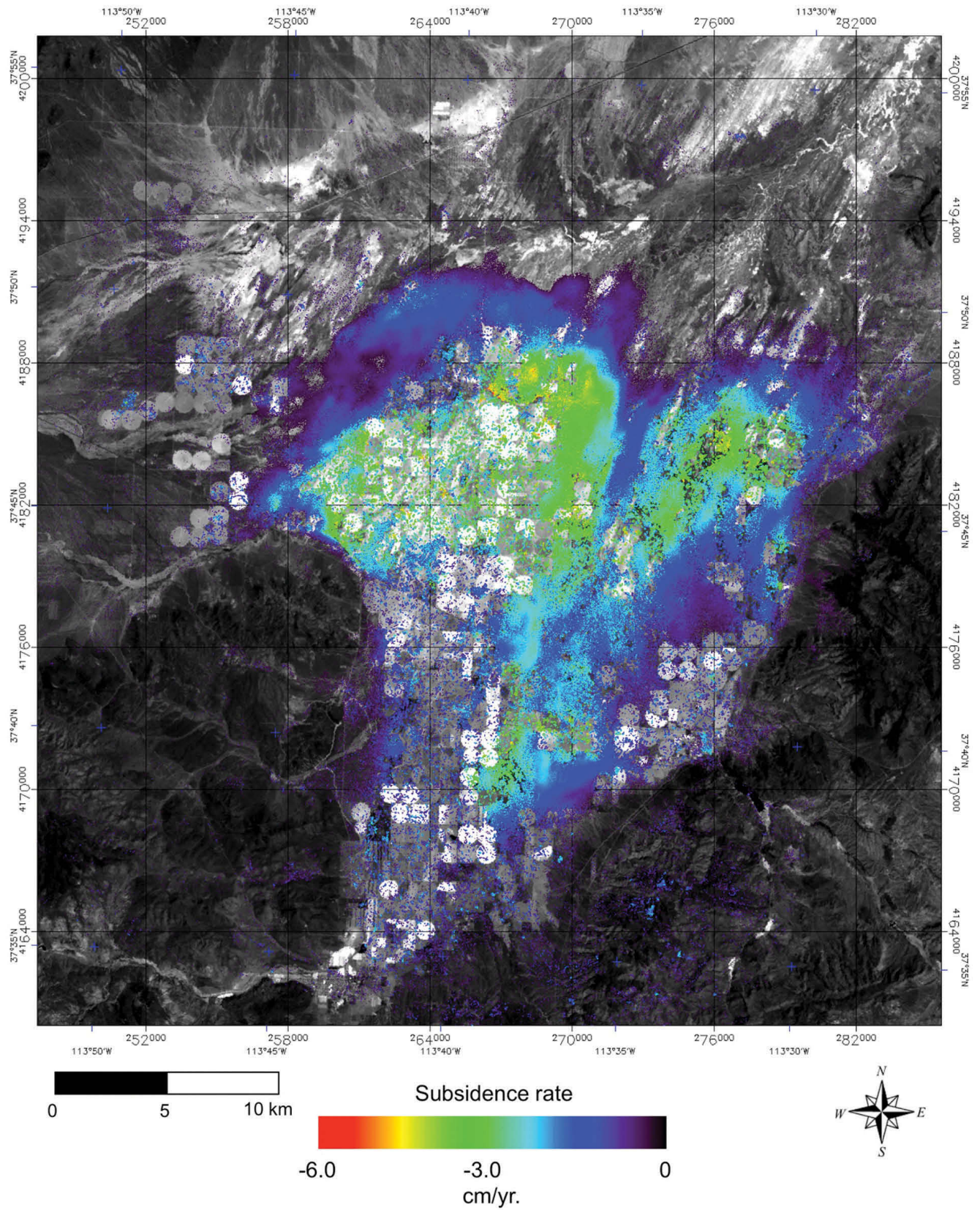


**Figure 14a.** Subsidence rate map of the Escalante Valley from InSAR pair 4/21/1998–11/2/1999 as color over Landsat ETM+ band 4 in gray-scale. Negative values indicate surface lowering relative to bedrock. Color is the extent of the usable data.

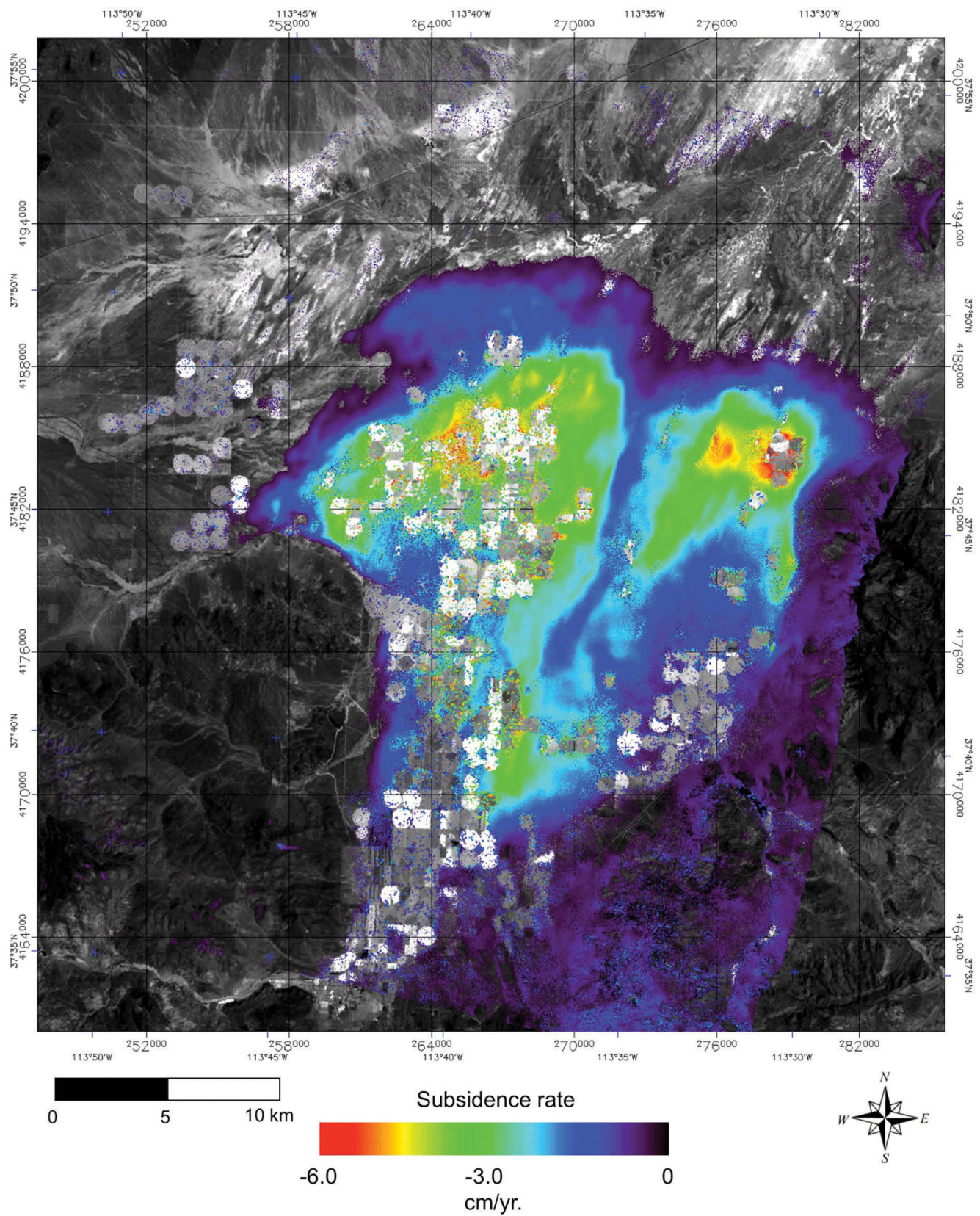


**Figure 14b.** Subsidence rate map of the Escalante Valley from InSAR pair 11/2/1999–10/17/2000 as color over Landsat ETM+ band 4 in gray-scale. Negative values indicate surface lowering relative to bedrock. Color is the extent of the usable data.

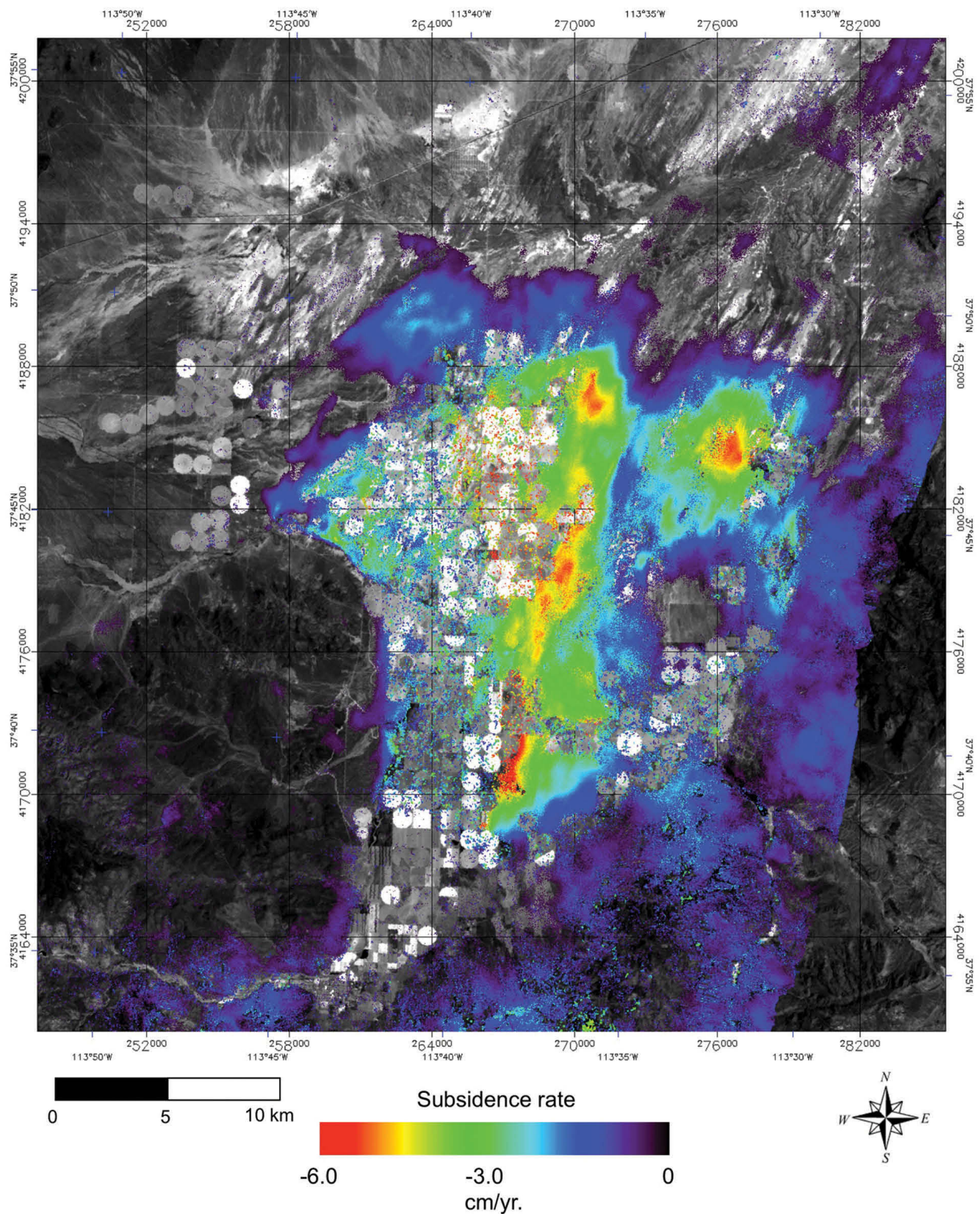


**Figure 14c.** Subsidence rate map of the Escalante Valley from InSAR pair 10/26/2004–11/15/2005 as color over Landsat ETM+ band 4 in gray-scale. Negative values indicate surface lowering relative to bedrock. Color is the extent of the usable data.

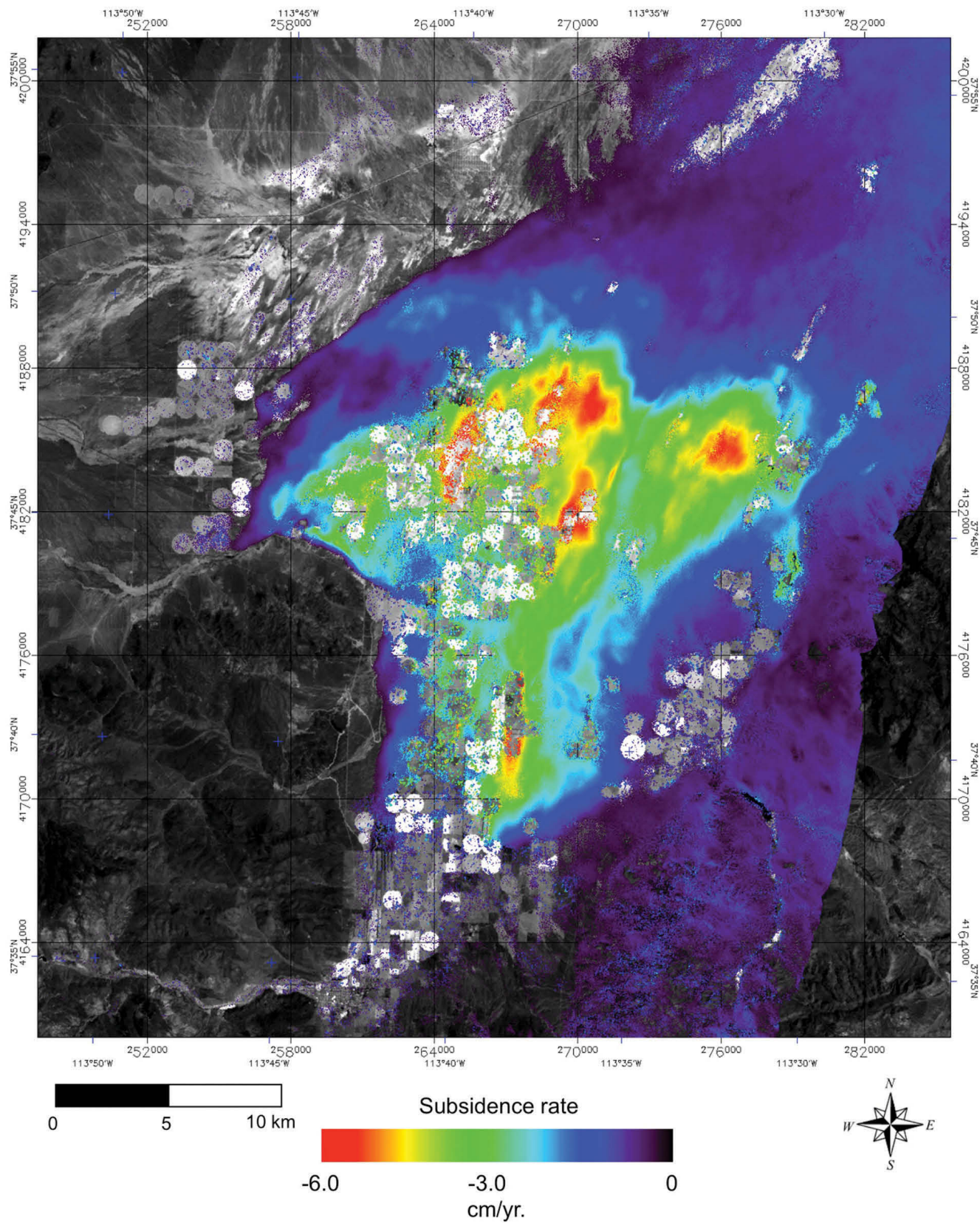


**Figure 14d.** Subsidence rate map of the Escalante Valley from InSAR pair 10/11/2005–12/5/2006 as color over Landsat ETM+ band 4 in gray-scale. Negative values indicate surface lowering relative to bedrock. Color is the extent of the usable data.

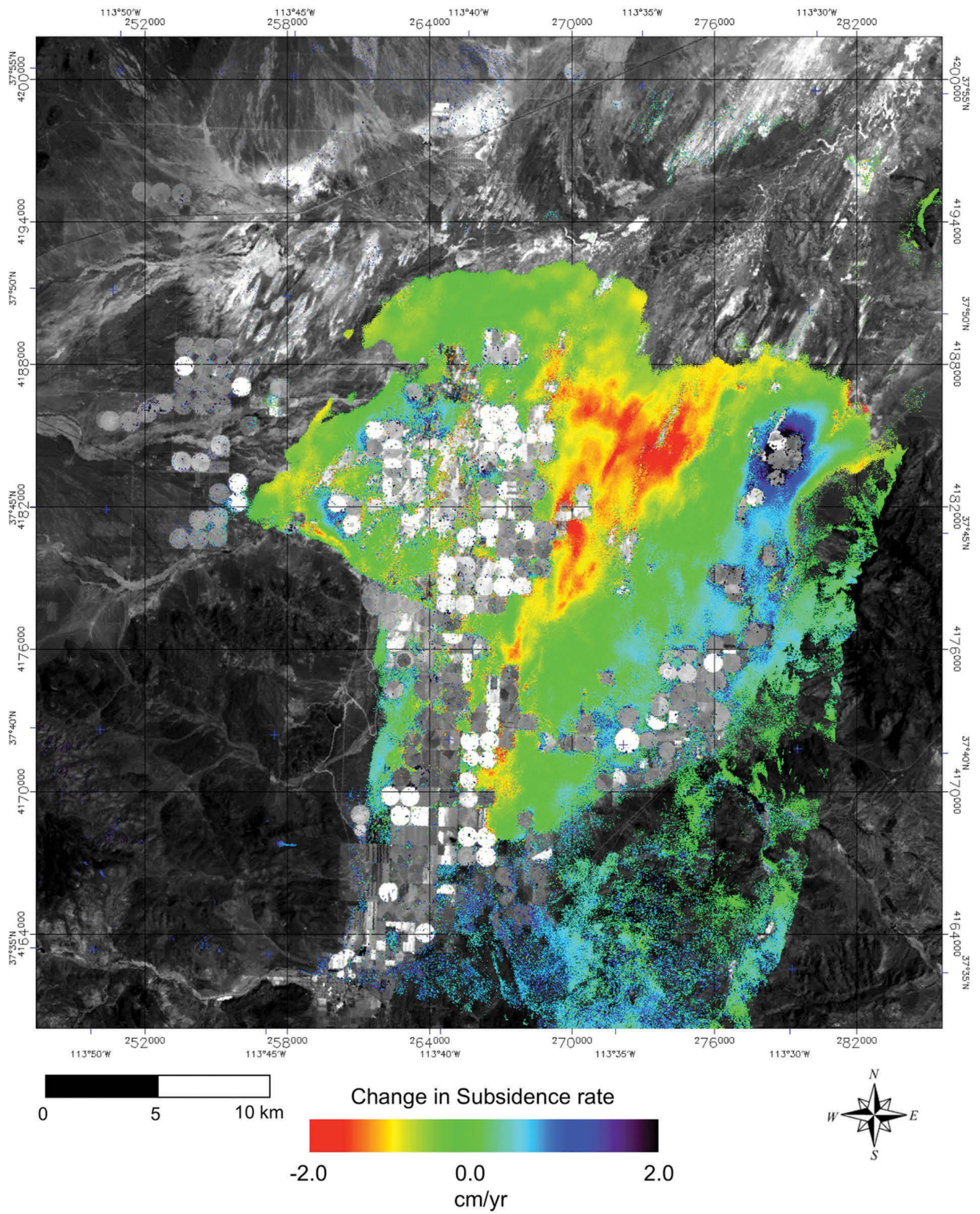


**Figure 15a.** Change in subsidence rate of the Escalante Valley from subtracting figure 14b (11/2/1999 to 10/17/2000) from figure 14d (10/11/2005 to 12/5/2006 ). Negative values are increasing subsidence rates over time and positive values are decreasing subsidence rates.

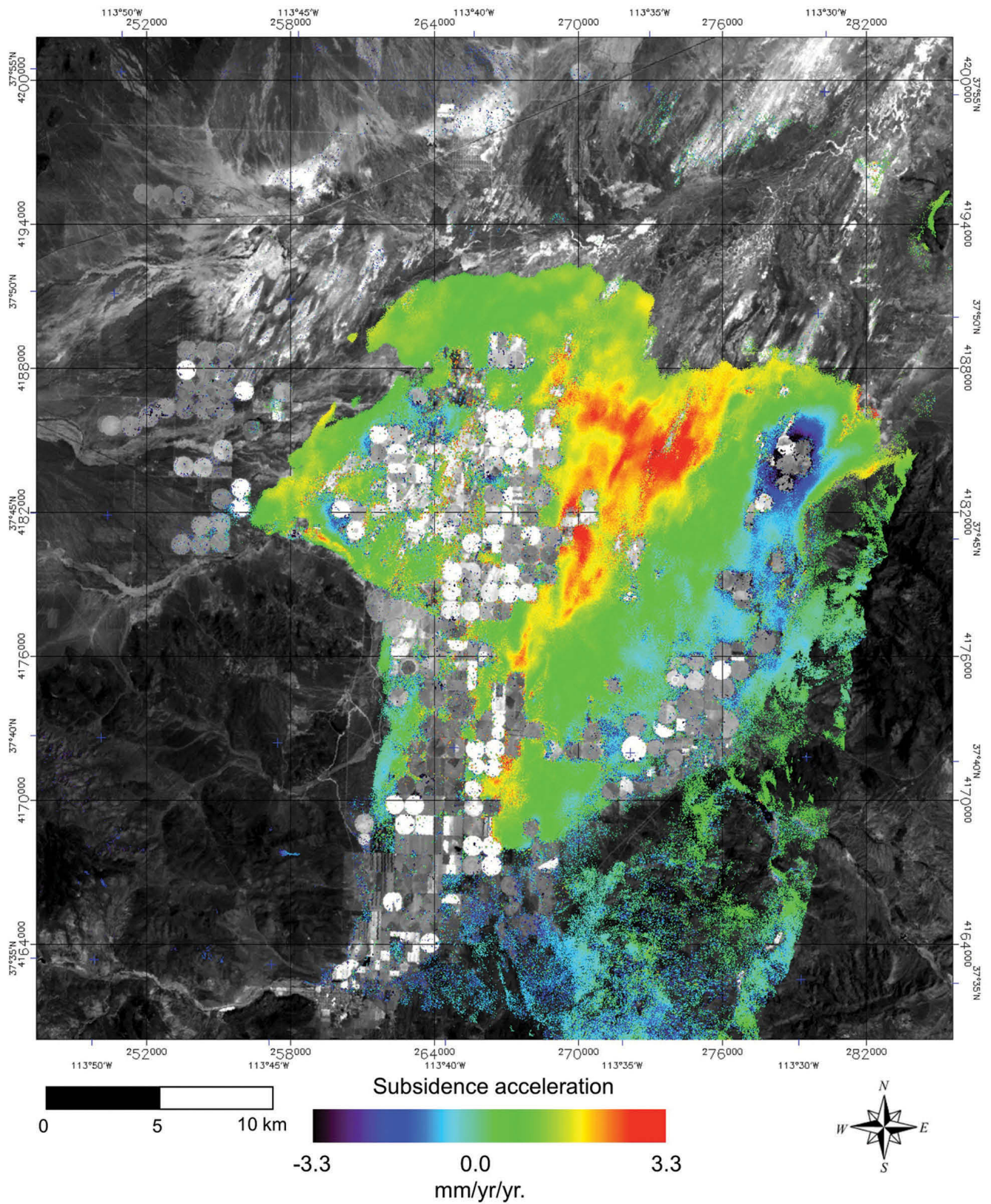


**Figure 15b.** Acceleration of subsidence in the Escalante Valley from subtracting figure 14b (11/2/1999 to 10/17/2000) from figure 14d (10/11/2005 to 12/5/2006) and dividing by the time interval (6 years). Positive values are increasing subsidence rates over time (accelerating) and negative values are decreasing subsidence rates (decelerating).

14a) was not used because of the large areas without data due to low coherence. For the change in subsidence rate image, a negative value indicates the subsidence is increasing over time (red and yellow) and positive values are areas where the subsidence rate has decreased (blue) (figure 15a). The green areas are where there has been little or no change in the subsidence rate. The area of increasing subsidence is larger than that of decreasing subsidence. The magnitude of increasing subsidence is also greater, up to 2 cm/yr increase, than the maximum decrease of 1 cm/yr. The dark blue areas of maximum subsidence decrease are on the perimeter of data holes (due to crop growth), which surround circular irrigation fields (figure 15a) with wells in their center (figure 13b). It seems likely these wells decreased water withdrawal during the time period 11/2/1999–10/17/2000 to 10/11/2005–12/5/2006 and the aquifer is responding elastically. The areas of increasing subsidence do not all coincide with circular irrigation fields or water wells (figure 15a). The NNE-SSW trending ridge of reduced subsidence seen in the individual subsidence rate maps (figure 14) shows an increasing subsidence, indicating the areas affected by subsidence are expanding. There are also locations of increasing subsidence coinciding with individual circular fields and wells, probably indicating the water withdrawals are increasing. It could also imply the aquifer is now responding inelastically, but this is unlikely considering the areas of decreasing subsidence, which are responding elastically, are within 5 km (figure 15a).

The rate at which the subsidence rate is changing over time is shown as the acceleration of the subsidence (figure 15b). This is over the same time period as figure 15a and shows the identical spatial pattern, the difference being the units, which are now in acceleration (mm/yr/yr). Positive values are increasing subsidence rates and negative values are decreasing subsidence rates. The maximum acceleration is 3.3 mm/yr/yr. If this acceleration continues for the next ten years subsidence rates will be 9.3 cm/yr in these areas in 2016. The accumulated subsidence from 1998 to 2016 under this scenario can be estimated from the sum of the subsidence maps for the measured years (figure 13), plus the estimated subsidence for the missing years 2000 to 2004, plus the extrapolated subsidence assuming acceleration of 3.3 mm/yr/yr (figure 15b). Since there are no satellite data between 2000 and 2004, the rate during this time is assumed to be constant at the 1999 to 2000 rate of 5.0 cm/yr. These data predict the maximum accumulated subsidence from 1998 to 2016 will be 1.17 m. Subsidence of greater than a meter due to groundwater withdrawal has also been measured in California (Ikehara and Phillips, 1994; Bertoldi and others, 1991).

## CONCLUSIONS AND RECOMMENDATIONS

The persistent scatterer InSAR (PSInSAR) technique was not successful in the Escalante Valley due to too few and too widely spaced persistent scatterers. Features that did form PS clusters were metal buildings surrounded by gravel/bare ground and metal power line towers. Features that did not classify as PS were buildings surrounded by vegetation, buildings without side walls, or buildings constructed during the time series of SAR images. Therefore, PS techniques may be more useful in urban or more developed areas.

Nearly annual subsidence rate maps can be constructed that include a large portion of the Escalante Valley from traditional InSAR with MCF unwrapping. The subsidence rate in the north central portion of the valley increased from 1998 to 2006. This area of subsidence has been mapped on all InSAR displacement maps back to 1993 (Forster, 2006). A previously unmapped area of subsidence in the southern end of the valley began to appear in 1999 then increased and persisted to the latest mapping in 2006. The extent of subsidence is expanding and the subsidence rates are accelerating in most areas, although decelerating subsidence surrounds some water wells. The projected accumulated subsidence from 1998 to 2016 for the areas of maximum subsidence is greater than one meter.

SAR data acquired from ENVISAT over the coming years could be used to monitor the current trend of increasing magnitude of subsidence and expansion of the area experiencing subsidence in the Escalante Valley. Future analysis could also be used to evaluate subsidence mitigation strategies.

## ACKNOWLEDGMENTS

Funding for this study was provided by the Utah Geological Survey. The SAR data were purchased from Eurimage through ERC-146.

## REFERENCES

- Amelung, F., Galloway, D.L., Bell, J.W., Zebker, H.A., and Lacznak, R.J., 1999, Sensing the ups and downs of Las Vegas—InSAR reveals structural control of land subsidence and aquifer-system deformation: *Geology*, v. 27, p. 483–486.
- Bawden, G.W., Thatcher, W., Stein, R.S., Hudnut, K.W., and Peltzer, G., 2001, Tectonic contraction across

- Los Angeles after removal of groundwater pumping effects: *Nature*, v. 412, p. 812–815.
- Bertoldi, G.L., Johnston, R.H., and Evenson, K.D., 1991, Ground water in the Central Valley, California—a summary report: U.S. Geological Survey Professional Paper 1401-A., 44 p.
- Burgmann R., Hilley, G., Ferretti, A., and Novali, F., 2006, Resolving vertical tectonics in the San Francisco Bay Area from permanent scatterer InSAR and GPS analysis: *Geology* v. 34, p. 221–224.
- Colesanti, C., Ferretti, A., Novali, F., Prati, C., and Rocca, F., 2003a, SAR monitoring of progressive and seasonal ground deformation using the permanent scatterers technique: *IEEE Transactions on Geoscience and Remote Sensing*, v. 41, n. 7, p. 1685–1701.
- Colesanti, C., Ferretti, A., Prati, C., and Rocca, F., 2003b, Monitoring landslides and tectonic motions with the permanent scatterers technique: *Engineering Geology*, v. 68, p. 3–14.
- Costantini, M., 1998, A novel phase unwrapping method based on network programming: *IEEE Transactions on Geoscience and Remote Sensing*, v. 36, n. 3, p. 813–821.
- Dehls, J.F., 2005, Permanent scatterer InSAR processing: Forsmark, Geological Survey of Norway, Report Number 2005.83, 28 p.
- Ferretti, A., Prati, C., and Rocca, F., 2001, Permanent scatterers in SAR interferometry: *IEEE Transactions on Geoscience and Remote Sensing*, v. 39, n. 1, p.8–20.
- Forster, R., 2006, Land subsidence in southwest Utah from 1993 to 1998 measured with interferometric synthetic aperture radar (InSAR): Utah Geological Survey Miscellaneous Publication 06-5, p. 30.
- Galloway, D.L., Hudnut, K.W., Ingebritson, S.E., Phillips, S.P., Peltzer, G., Rogez, F., and Rosen, P.A., 1998, InSAR detection of systematic compaction and land subsidence in Antelope Valley, Mojave Desert, California: *Water Resources Research*, v. 34, p. 2573–2585.
- Galloway, D.L., Jones, D.R., and Ingebritsen, S.E., 2000, Measuring land subsidence from space: U.S. Geological Survey Fact Sheet 051-00, 4 p.
- Gamma Remote Sensing, 2007, Users guide Gamma Remote Sensing Software for processing InSAR data, <http://www.gamma-rs.ch/nc/software/>.
- Goldstein, R.M., Zebker, H.A., and Werner, C.L., 1988, Satellite radar interferometry—Two-dimensional phase unwrapping: *Radio Science*, v. 23, p. 713–720.
- Hilley, G.E., Bürgmann, R., Ferretti, A., Novali, F., and Rocca, F., 2004, Dynamics of slow-moving landslides from permanent scatterer analysis: *Science*, v. 304. n. 5679, p. 1952–1955.
- Hoffmann, J., Zebker, H.A., Galloway, D.L., and Amelung, F., 2001, Seasonal subsidence and rebound in Las Vegas Valley, Nevada, observed by synthetic aperture radar interferometry: *Water Resources Research*, v. 37, n. 6, p. 1551–1566.
- Hooper, A., Zebker, H., Segall, P., and Kampes, B., 2004, A new method for measuring deformation on volcanoes and other natural terrains using InSAR persistent scatterers: *Geophys. Res. Lett.*, 31, L23611, doi:10.1029/2004GL021737.
- Ikehara, M.E., and Phillips, S.P., 1994, Determination of land subsidence related to ground-water level declines using global positioning system and leveling surveys in Antelope Valley, Los Angeles and Kern Counties, California, 1992: United States Geological Survey Water-Resources Investigations Report 94-4184, p. 101.
- Le Mouelic, S., Raucoules, D., Carnec, C., King, C., and Adragna, F., 2002, Ground uplift in the city of Paris (France) revealed by satellite radar interferometry: *Geoscience and Remote Sensing Symposium, IGARSS '02*, v. 2, p. 1222–1224.
- Lu, Z., and Danskin, W.R., 2001, InSAR analysis of natural recharge to define structure of a ground-water basin, San Bernardino, California: *Geophysical Research Letters*, v. 28, n. 13, p. 2661–2664.
- Lu, Z., Masterlark, T., Dzurisin, D., Rykhus, R., and Wicks, C., Jr., 2003, Magma supply dynamics at Westdahl volcano, Alaska, modeled from satellite radar interferometry: *Journal of Geophysical Research*, v. 108(B7), p. 2354, doi:10.1029/2002JB002311.
- Lund, W.R., DuRoss, C.B., Kirby, S.M., McDonald, G.N., Hunt, G., and Vice, G.S., 2005, The origin and extent of earth fissures in Escalante Valley, Southern Escalante Desert, Iron County, Utah: Utah Geological Survey Special Study 115, 29 p.
- Rosen, P., Hensley, S., Joughin, I.R., Li, F.K., Madsen, S.N., Rodriguez, E., and Goldstein, R.M., 2000, Synthetic aperture radar interferometry: *Proceedings of the IEEE*, v. 88, n. 3, p. 333–382.
- Strozzi, T., Wegmuller, U., Werner, C.L., Wiesmann, C.A., and Spreckels, V., 2003, JERS SAR interferometry for land subsidence monitoring: *IEEE Transactions on Geoscience and Remote Sensing*, v. 41, n. 7, p. 1702–1708.
- Werner, C., Wegmuller, U., Strozzi, T., and Wiesmann, A., 2003, Interferometric point target analysis for deformation mapping: *Geoscience and Remote Sensing Symposium. IGARSS '03. Proceedings*, v. 7, p. 4362–4364.